Physiological and morphological characterization of parvalbumin-containing interneurons of the rat basolateral amygdala

ARTICLE *in* THE JOURNAL OF COMPARATIVE NEUROLOGY · SEPTEMBER 2006

Impact Factor: 3.23 · DOI: 10.1002/cne.21049 · Source: PubMed

THE JOURNAL OF COMPARATIVE NEUROLOGY 498:142–161 (2006)

Physiological and Morphological Characterization of Parvalbumin-Containing Interneurons of the Rat Basolateral Amygdala

DONALD GORDON RAINNIE,[1]* IRAKLI MANIA,[1] FRANCO MASCAGNI,[2] AND ALEXANDER JOSEPH McDONALD[2]

[1]Department of Psychiatry and Center for Behavioral Neuroscience, Yerkes National Primate Research Center, Emory University School of Medicine, Atlanta, Georgia 30329
[2]Department of Pharmacology, Physiology, and Neuroscience, University of South Carolina School of Medicine, Columbia, South Carolina 29208

ABSTRACT

The basolateral amygdala (BLA) is critical for the generation of emotional behavior and the formation of emotional memory. Understanding the neuronal mechanisms that contribute to emotional information processing in the BLA will ultimately require knowledge of the anatomy and physiology of its constituent neurons. Two major cell classes exist in the BLA, pyramidal projection neurons and nonpyramidal interneurons. Although the properties of projection neurons have been studied in detail, little is known about the properties of BLA interneurons. We have used whole-cell patch clamp recording techniques to examine the physiological properties of 48 visually identified putative interneurons from the rat anterior basolateral amygdalar nucleus. Here, we report that BLA interneurons can be differentiated into four electrophysiologically distinct subtypes based on their intrinsic membrane properties and their response to afferent synaptic input. Interneuron subtypes were named according to their characteristic firing pattern generated in response to transient depolarizing current injection and were grouped as follows: 1) burst-firing interneurons (n = 13), 2) regular-firing interneurons (n = 11), 3) fast-firing interneurons (n = 10), and 4) stutter-firing interneurons (n = 14). Post hoc histochemical visualization confirmed that all 48 recorded neurons had morphological properties consistent with their being local circuit interneurons. Moreover, by using triple immunofluorescence (for biocytin, calcium-binding proteins, and neuropeptides) in conjunction with patch clamp recording, we further demonstrated that over 60% of burst-firing and stutter-firing interneurons also expressed the calcium-binding protein parvalbumin (PV^+). These data demonstrate that interneurons of the BLA show both physiological and neurochemical diversity. Moreover, we demonstrate that the burst- and stutter-firing patterns positively correlate with PV^+ immunoreactivity, suggesting that these neurons may represent functionally distinct subpopulations. J. Comp. Neurol. 498: 142–161, 2006.

Indexing terms: electrophysiology; immunohistochemistry; calcium-binding protein; synchrony

The basolateral amygdala (BLA) is critical for the generation of emotional behavior and the formation of emotional memories (Aggleton, 1992, 2000). Understanding the neuronal mechanisms mediating emotional information processing in the BLA will ultimately require knowledge of the anatomy and physiology of its constituent neurons. Previous studies have shown that there are two major cell classes in the BLA, pyramidal neurons and nonpyramidal neurons. Although these cells do not exhibit a laminar organization, their morphology, synaptology, electrophysiology, and pharmacology are remarkably similar to those of their counterparts in the cerebral cortex (McDonald, 1992; Washburn and Moises, 1992b; Rainnie et al., 1993; Pare et al., 2003). Thus, the principal neurons

Grant sponsor: National Institutes of Health; Grant number: NS38998 (to A.J.M.); Grant number: MH069852 (to D.G.R.); Grant sponsor: National Alliance for Research on Schizophrenia and Depression (to D.G.R.); Grant sponsor: Center for Behavioral Neuroscience STC Program, NSF Agreement; Grant number: IBN-9876754.

*Correspondence to: Don Rainnie, Assistant Professor, Department of Psychiatry and Center for Behavioral Neuroscience, Emory University, Yerkes Neuroscience Building, Room 5220, 954 Gatewood Road, Atlanta, GA 30329. E-mail: drainni@emory.edu

Received 28 September 2005; Revised 6 January 2006; Accepted 31 March 2006

DOI 10.1002/cne.21049

Published online in Wiley InterScience (www.interscience.wiley.com).

in the BLA are pyramidal-like projection neurons with spiny dendrites that utilize glutamate as an excitatory neurotransmitter (Fuller et al., 1987; McDonald, 1992, 1996). In contrast, most nonpyramidal neurons in the BLA are spine-sparse interneurons that utilize γ-aminobutyric acid (GABA) as an inhibitory neurotransmitter (McDonald, 1982; Carlsen, 1988; McDonald and Pearson, 1989).

As in the cerebral cortex, subpopulations of GABAergic interneurons in the BLA contain calcium-binding proteins [parvalbumin (PV), calbindin (CB), and calretinin (CR)] and neuropeptides (vasoactive intestinal peptide, somatostatin, neuropeptide Y, and cholecystokinin; McDonald and Pearson, 1989; Kemppainen and Pitkänen, 2000; McDonald and Mascagni, 2001a; Levita et al., 2003b). The results of recent double-labeling studies suggest that the rat BLA contains at least four distinct subpopulations of interneurons: 1) PV^+/CB^+ neurons, 2) somatostatin$^+/CB^+$ neurons, 3) large multipolar cholecystokinin$^+$ neurons that are often CB^+, and 4) small bipolar and bitufted interneurons that exhibit extensive colocalization of vasoactive intestinal peptide, CR, and cholecystokinin (Kemppainen and Pitkänen, 2000; McDonald and Mascagni, 2001a, 2002; McDonald and Betette, 2001). Similar subpopulations of GABAergic interneurons have been identified in the cerebral cortex, where it has been demonstrated that each subpopulation may exhibit characteristic electrophysiological properties as a result of the expression of distinct sets of ion channels (Kawaguchi and Kondo, 2002; Markram et al., 2004).

Because of this diversity, activation of subpopulations of interneuron is no longer perceived as simply preventing projection neurons from firing. At the cellular level, interneuron functions include governing action potential generation, firing pattern, membrane potential oscillations, and dendritic calcium spikes (Cobb et al., 1997; Fricker and Miles, 2001). At the network level, GABAergic interneurons are important in controlling synaptic strength and synchronizing neuronal population activity (Cobb et al., 1995; Acsady et al., 1996; Pouille and Scanziani, 2001). Hence, far from simply inhibiting projection neurons, neocortical interneurons are a major driving force in establishing spatiotemporal encoding. Surprisingly, there have been no studies directly examining the electrophysiological properties of distinct subpopulations of interneurons in the BLA.

Interneurons expressing PV are a critical component of the inhibitory circuitry in the BLA. As in the cortex, many PV^+ interneurons in the BLA appear to be basket or chandelier cells (axoaxonal cells; Pitkänen and Amaral, 1994; Sorvari et al., 1995; McDonald and Betette, 2001). These cells constitute about 50% of the GABAergic interneurons in the BLA and provide a strong perisomatic inhibition of local pyramidal neurons (PNs; McDonald and Mascagni, 2001a; McDonald and Betette, 2001). Moreover, most excitatory afferent input onto PV^+ interneurons arise from local axon collaterals of BLA projection neurons (Smith et al., 2000), and individual projection neurons make multiple perisomatic contacts with PV^+ interneurons (McDonald et al., 2005), suggesting that the activities of these two cell populations are tightly regulated by this powerful reciprocal circuit. Significantly, in the basolateral complex, PV^+ interneurons are also the primary interneuronal target for axon terminals arising from brainstem dopamine neurons (Asan, 1998; Brinley-Reed and McDonald, 1999), and dopaminergic regulation of inhibitory gating in the BLA attenuates prefrontal cortical suppression of sensory input (Rosenkranz and Grace, 2001) and facilitates the induction of long-term potentiation (LTP; Bissiere et al., 2003). If we are to understand the mechanisms by which dopamine, and other neurotransmitters, can regulate inhibitory gating in the BLA, we must first determine the physiological properties of the interneurons mediating the gating response. Consequently, in the present investigation, we have combined whole-cell patch clamp recording with immunohistochemistry to study directly the electrophysiological properties of this important interneuron subpopulation.

MATERIALS AND METHODS

In vitro slice recording techniques

Adult male Sprague-Dawley (26–40 days; Charles River, Cambridge, MA) rats were used for in vitro patch clamp recording experiments. Every effort was used to minimize both animal suffering and the number of animals used in these experiments. All experimental protocols strictly conform to National Institutes of Health guidelines for the care and use of laboratory animals and were approved by the Institutional Animal Care and Use Committee of Emory University.

In vitro whole-cell patch clamp recording

Slices of 350 μm thickness containing the anterior basolateral nucleus (Bregma levels −2.0 to −3.0) were obtained as described previously (Rainnie, 1999a). Briefly, the brains of anesthetized rats were rapidly dissected and immersed in a cold (4°C) oxygenated artificial cerebrospinal fluid (ACSF) "cutting solution," of the following composition (in mM): NaCl (130), $NaHCO_3$ (30), KCl (3.50), KH_2PO_4 (1.10), $MgCl_2$ (6.0), $CaCl_2$ (1.0), glucose (10), supplemented with kynurenic acid (2.0). A low-calcium high-magnesium ASCF, supplemented with the nonspecific glutamate receptor antagonist kynurenic acid, was used during tissue slicing to minimize glutamate-induced neurotoxicity. After sectioning, slices were maintained at 32°C in "cutting solution" oxygenated with a mixture of 95% oxygen and 5% carbon dioxide for 1 hour prior to recording. Slices were then transferred to a holding chamber containing "control" ACSF maintained at room temperature, with the following composition (in mM): NaCl (130), $NaHCO_3$ (30), KCl (3.50), KH_2PO_4 (1.10), $MgCl_2$ (1.30), $CaCl_2$ (2.50), and glucose (10). When required, slices were transferred to a Warner Series 20 submersion-type slice chamber (0.5 ml volume; Warner Instruments, Hamden, CT) mounted on the stage of a Leica DM-LFS microscope (Leica Microsystems Inc., Bannockburn, IL) and continuously perfused by gravity-fed oxygenated "control" ACSF heated to 32°C. Slices were perfused at a rate of 1–2 ml/minute and viewed by using differential interference contrast (DIC) optics and infrared (IR) illumination with an IR-sensitive CCD camera (Orca ER; Hamamatsu, Tokyo, Japan). Whole-cell patch clamp recordings were obtained by using standard techniques (Rainnie, 1999a; Rainnie et al., 2004; McDonald et al., 2005). Thin-walled borosilicate glass patch electrodes (WPI, Sarasota, FL) were filled with (in mM): K-gluconate (130), phosphocreatinine (5), KCl (3), HEPES (10), $MgCl_2$ (3), MgATP (2), NaGTP (0.2), and 0.35% biocytin, adjusted

to pH 7.3 with KOH and having an osmolarity of 280–290 mOsm. Electrode resistances ranged from 5 to 8 MΩ. Whole-cell access resistances measured in voltage clamp were in the range 5–20 MΩ and were monitored during the course of each experiment; a change of 15% was deemed acceptable.

Identification of BLA interneurons

Individual BLA interneurons were visualized in situ by using DIC microscopy in combination with a ×40 water-immersion objective (Leica Microsystems Inc.) and displayed in real time on a computer monitor via Simple PCI acquisition software (Compix, Inc.). For this study, specific morphological criteria were used to preselect putative interneurons in the visual field. Hence, only those neurons having a somatic diameter of less than 15 μm, which were either spherical or fusiform in appearance, were selected as putative interneurons. Interneurons were identified according to their characteristic size and shape and were located between 50 and 100 μM beneath the surface of the slice. Whole-cell recordings were made with an Axopatch-1D amplifier (Molecular Devices Corporation, Sunnyvale, CA) by using pClamp 9.0 software and a Digidata 1320 A-D interface (Molecular Devices Corporation). All whole-cell potentials/currents were elicited from a holding potential of −60 mV unless otherwise stated.

Electrophysiological characterization of BLA interneurons

Results from previous intracellular and "blind" whole-cell patch clamp studies of putative BLA interneurons suggested that these neurons could be distinguished from projection neurons in that they have a significantly higher membrane input resistance (Rm >100 MΩ; Rainnie et al., 1993; Rainnie, 1999a), fire at frequencies >20 Hz for the duration of a depolarizing current injection, and show little or no spike frequency adaptation or accommodation in response to prolonged (750 msec) depolarizing current injection (Mahanty and Sah, 1998; Rainnie, 1999a). However, none of these studies examined the potential correlation between the neurochemical phenotype of the recorded interneurons and their physiological properties.

In this study, at the start of each experiment, putative interneurons were visually identified, and then standardized protocols were performed in current clamp to validate further the identity of recorded neurons as being putative BLA interneurons. The membrane properties of each neuron were first examined at its resting membrane potential (Vm) and then at −60 mV by using DC current injection to standardize comparisons between putative interneurons. Here, transient (750 msec) hyperpolarizing current steps of increasing amplitude (50–250 pA) were used to determine the input resistance (Rm) and also to determine the presence or absence of any voltage-dependent currents that may be activated upon membrane hyperpolarization. Membrane input resistance was calculated from the peak voltage deflection obtained in response to the first −50-pA step in each series of current steps, to minimize the effects of voltage-dependent currents on Rm. Next, transient (750 msec) depolarizing current steps of increasing amplitude (range 25–250 pA) were used to determine the firing properties of putative interneurons. This protocol was also used to determine the 10–90% rise time, and spike width at half-peak amplitude, for each action potential generated in response to depolarizing current injection. For each cell recorded, the average rise time and spike width were calculated from the sum of all the evoked action potentials in the series of depolarizing current steps.

Putative interneurons were also examined for the presence, or absence, of postspike afterhyperpolarizing potentials (AHPs) following repetitive action potential discharge. Here, the peak AHP amplitude and AHP duration were plotted as a function of the number of spikes generated in response to a maximal 250-pA current step in Graphpad Prism 4.0 software (Graphpad Software, San Diego, CA). For each condition, the correlation coefficient was calculated at the 95% confidence level.

During the course of our experiments, it became apparent that PV^+ interneurons of the BLA fall into two distinct electrophysiological categories based on their response to depolarizing current injection. Hence, a subset of putative interneurons was recorded in voltage clamp mode to examine the current–voltage relationship of their intrinsic membrane currents. Here, steady-state currents were determined by using voltage commands that "ramped" the membrane potential from −100 to −40 mV at a rate of 10 $mV/second^{-1}$.

Statistical analysis

Statistical significance for all electrophysiological data was determined by using an unpaired Student's *t*-test with a confidence limit set at 95%, unless otherwise stated.

Immunohistochemical analysis

Slices (n = 48) were fixed overnight in 4% paraformaldehyde in 0.1 M phosphate buffer (PB; pH 7.4) and then resectioned at 75 μm on a vibratome. Sections were processed for immunohistochemistry in wells of tissue culture plates. All antibodies were diluted in phosphate-buffered saline (PBS; pH 7.4) containing 0.5% Triton X-100 and 1% normal goat serum. Sections were incubated in a cocktail of mouse anti-PV antibody (1:1,000–1:4,000; Sigma, St. Louis, MO) and either rabbit anti-vasoactive intestinal polypeptide (1:400; ImmunoStar Inc; Hudson, WI) or rabbit anti-CR (1:750; Chemicon, Temecula, CA) antibodies overnight at 4°C. Sections were then incubated in a cocktail of Alexa-488-conjugated goat anti-mouse IgG (1:400; Molecular Probes, Eugene, OR) and Alexa-660-conjugated goat anti-rabbit IgG (1:400; Molecular Probes) for 3 hours at room temperature, followed by incubation in Alexa-568-conjugated streptavidin (1:4,000; Molecular Probes) for 3 hours for biocytin visualization, and then coverslipped with Vectashield mounting medium (Vector Laboratories, Burlingame, CA). Sections were examined with a Bio-Rad MRC-1024 confocal laser scanning microscope equipped with an argon-krypton laser attached to a Nikon Optiphot fluorescence microscope. Fluorescence of Alexa 488 (green), Alexa 568 (red), and Alexa 660 (far red) dyes was analyzed by using filter configurations for sequential excitation/imaging via 488 nm, 568 nm, and 647 nm channels. Biocytin-filled neurons that were not immunostained in the first round of staining were subjected to a second round of immunofluorescence staining for somatostatin and cholecystokinin. Light micrographic images were obtained by using a Micropublisher 5.0 digital CCD camera (Q-Imaging Corp., Austin, TX). Both light and confocal digital images were adjusted for brightness and contrast in Photoshop 6.0.

After immunofluorescence identification of neuronal phenotype, sections were removed from slides, incubated in 0.3% hydrogen peroxide (30 minutes) to eliminate staining of red blood cells, incubated in Elite ABC reagent (Vector Laboratories) for 3 hours, and stained by using nickel-intensified 3,3′-diaminobenzidine-4HCl (DAB; Sigma) as a chromogen (McDonald et al., 2005). Sections were then mounted on gelatinized slides, dried overnight, dehydrated in ethanols, cleared in xylene, and coverslipped with Permount (Fisher Scientific, Pittsburgh, PA). In addition, sections from some neurons were counterstained with cresyl violet prior to coverslipping. Sections were analyzed with an Olympus BHA light microscope. Some neurons were drawn at ×630 magnification with a drawing tube.

Antibody specificity

The mouse monoclonal PV antibody utilized in this study (Sigma No. P3088, clone PARV-19) is one of the most widely used PV antisera in studies of the central nervous system. The immunogen used to generate the antibody was frog muscle PV. Studies conducted by the manufacturer indicate that it recognizes PV in a Ca^{2+} ion-dependent manner and does not react with other members of the EF-hand family, such as calmodulin, intestinal calcium-binding protein, S100A2 (S100L), S100A6 (calcyclin), or the α or β chain of S-100.

The antisera to vasoactive intestinal polypeptide (No. 20077; ImmunoStar, Inc.) was generated in a rabbit against porcine vasoactive intestinal polypeptide conjugated to bovine thyroglobulin with carbodiimide. The specificity of the antiserum was examined by the manufacturer by soluble preadsorption of vasoactive intestinal polypeptide at a concentration of 10^{-5} M; vasoactive intestinal polypeptide immunolabeling was completely abolished. Preadsorption with the following peptides resulted in no reduction of immunostaining: secretin, gastric inhibitory polypeptide, somatostatin, glucagon, insulin, adrenocorticotropic hormone, gastrin 34, FMRF-amide, rat GHRF, human GHRF, peptide histidine isoleucine 27, rat pancreatic polypeptide, motilin, peptide YY, substance P, neuropeptide Y, and calcitonin gene-related peptide. Preadsorption of this antiserum in our laboratory with vasoactive intestinal polypeptide (Sigma) at a concentration of 100 μg/ml also abolished all tissue staining; preadsorption with somatostatin-14, neuropeptide Y, and cholecystokinin-8 (all obtained from Sigma) had no effect. The CR antiserum (No. AB5054; Chemicon) was raised in rabbit against recombinant rat CR and recognizes both calcium-bound and calcium-unbound conformations of CR in immunoblots performed by the manufacturer. It is a widely used antiserum that produces the characteristic pattern for CR staining of bipolar interneurons in the cortex and BLA (Jacobowitz and Winsky, 1991).

The cholecystokinin antibody (1:500; monoclonal antibody No. 9303, generously donated by Dr. J.H. Walsh, UCLA) was raised against gastrin, but recognizes cholecystokinin because of homologies in the terminal pentapeptide shared by these peptides. Gastrin is not found in the telencephalon, and this antibody has been used in numerous studies of the forebrain to study the distribution of cholecystokinin (see McDonald and Mascagni, 2001b). Preadsorption of this antibody with CCK-8 (25 μg/ml; Sigma) abolished all immunostaining in the amygdala and other forebrain regions (McDonald and Mascagni, 2001b). The somatostatin antibody (1:500; No. IHC-8004; Peninsula Laboratories Inc., Belmont, CA) was raised in rabbit against somatostatin-28. Studies conducted by the manufacturer have demonstrated reactivity for somatostatin-28 and somatostatin-25 but no cross-reactivity for substance P, cholecystokinin, or vasoactive intestinal polypeptide. Staining in the amygdala appeared to be identical to that obtained with a well-characterized monoclonal antibody to somatostatin that recognizes somatostatin-28 and somatostatin-14 (McDonald and Mascagni, 2002).

RESULTS

Morphological identification of BLA interneurons

In this study, we recorded the physiological properties of 48 putative BLA interneurons, which were chosen based on their morphological criteria (see Materials and Methods). Studies in the neocortex using combined electrophysiological and immunohistochemical techniques to examine the physiological properties of interneurons have reported that prolonged dialysis with recording solutions could markedly diminish cytosolic levels of calcium-binding proteins and neuropeptides, resulting in an increase in false-negative staining (Kawaguchi, 1995). Consequently, the duration of each recording was kept to the minimum time necessary to obtain a clear physiological profile (mean duration 16.4 ± 1.5 minutes). Immunofluorescence and light microscopic analysis demonstrated that all 48 of the biocytin-filled neurons were spine-sparse, nonpyramidal interneurons (McDonald, 1982; Millhouse and DeOlmos, 1983). Somata and dendrites of these neurons appeared to be completely filled with biocytin, but the extent of axonal filling was variable.

Electrophysiological characterization of BLA interneurons

On the basis of our electrophysiological data alone, BLA interneurons were divided into four broad categories (Fig. 1). 1) Burst-firing neurons (BF; 13/48) had electrophysiological characteristics similar to those previously reported in our earlier "blind" patch clamp study (Rainnie, 1999a). Hence, in the absence of any exogenous current injection BF neurons were characterized by the occurrence of spontaneous bursts of action potentials (Fig. 1A–C, left trace; see also Fig. 3; Rainnie, 1999a). The bursts of actions potentials did not arise from the intrinsic properties of these neurons but were driven by rapidly summating high-frequency excitatory postsynaptic potentials (EPSPs; Rainnie, 1999a). However, in response to transient (750 msec) depolarizing current injection, BF interneurons typically elicited a short burst of action potentials that settled into a regular firing pattern, when not invaded by spontaneous bursts of action potentials driven by EPSPs. BF neurons also expressed a prominent depolarizing sag in the voltage response to transient hyperpolarizing current injection (Fig. 1B), which was blocked by inclusion in the extracellular ASCF of either cesium (6 mM; n = 4), or the specific I_h channel blocker ZD7288 (30 μM; n = 4; see Fig. 3C).

Regular-firing interneurons (RF; 11/48) share many of the same membrane properties as BF interneurons, such as a brief burst of action potentials, followed by a rela-

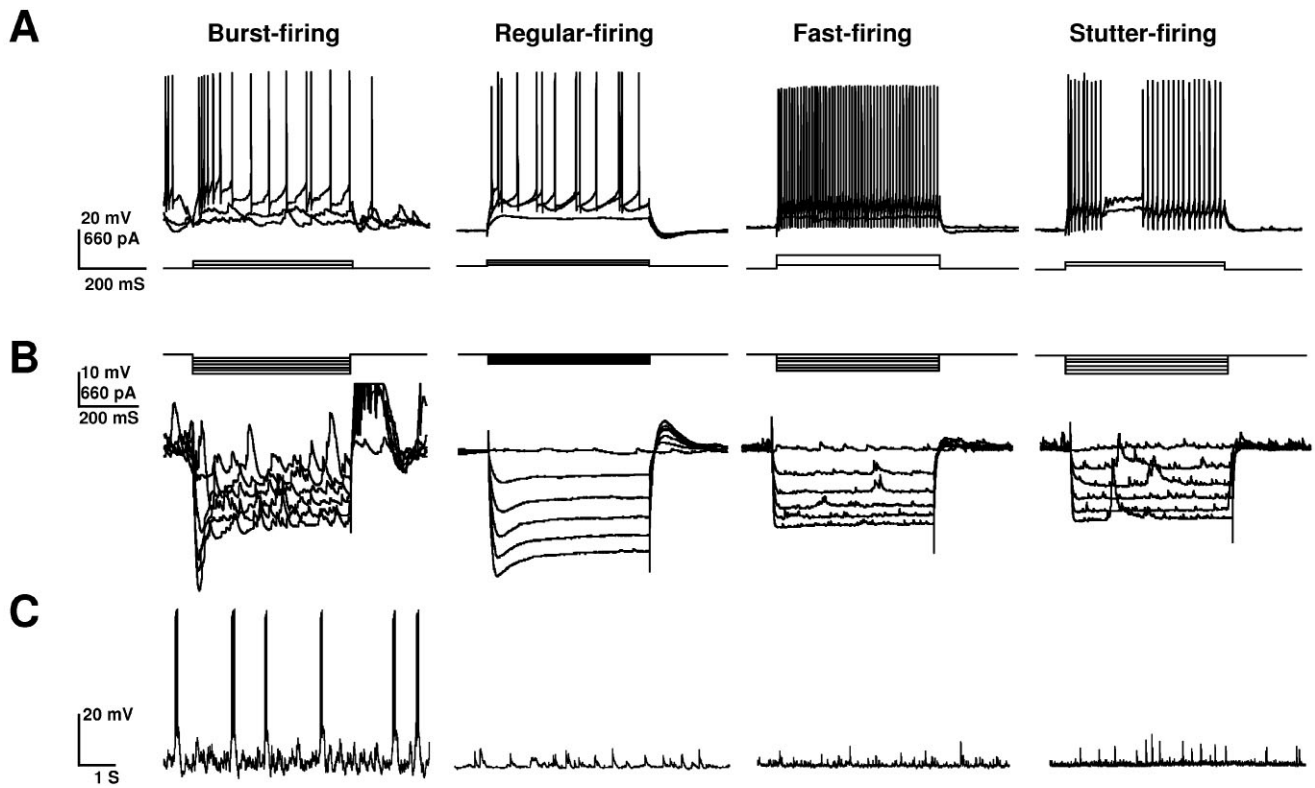

Fig. 1. Identification of four electrophysiologically distinct subtypes of BLA interneuron. Based on their action potential discharge pattern in response to depolarizing current injection (**A**), their voltage response to hyperpolarizing current injection (**B**), and their spontaneous synaptic activity (**C**), interneurons of the BLA can be subdivided into four subtypes; burst-firing, regular-firing, fast-firing, and stutter-firing.

tively rhythmic firing pattern in response to depolarizing current injection, and the presence of a prominent depolarizing sag in the voltage response to transient hyperpolarizing current injection (Fig. 1). However, although high-frequency spontaneous EPSPs were observed in RF interneurons, unlike the case for BF interneurons, spontaneous bursts of action potentials were never observed in RF interneurons. RF interneurons also had a significantly higher resting membrane input resistance (Rm) than BF neurons (RF = 449 ± 68 MΩ, n = 11; BF = 180 ± 51 MΩ, n = 13; $P < 0.005$).

Fast-firing interneurons (FF; 10/48) were distinct from both BF and RF interneurons (Fig. 2) in that they fired action potentials at high frequency throughout the duration of a 750-msec depolarizing current injection and showed no spike frequency adaptation or accommodation. In addition, FF interneurons typically displayed little or no I_h or rhythmic bursts of spontaneous EPSPs and showed a significantly lower input resistance than RF neurons (Rm = 138 ± 19 MΩ, n = 10, $P < 0.005$), but not BF or SF neurons ($P > 0.05$).

Stutter-firing interneurons (SF; 14/48) were similar in many ways to FF neurons in that they had a low Rm (135 ± 13 MΩ, n = 14) and typically displayed little or no I_h or rhythmic bursts of spontaneous EPSPs (Fig. 1). However, unlike FF interneurons, SF interneurons never fired a continuous train of action potentials in response to subthreshold depolarizing current injection but rather fired in a characteristic stutter-firing pattern. Here, depolarizing current injection elicited intermittent, high-frequency (100 Hz) trains of action potentials separated by brief periods of quiescence (see also Figs. 3, 6, inset).

Neurochemical identification of subpopulations of BLA interneurons: PV

Examination of the cytochemical phenotype of the 48 recovered interneurons by using triple immunofluorescence was performed to determine whether any of the electrophysiological profiles corresponded to a known cytochemical phenotype. Forty-three percent (21/48) of the recovered interneurons were immunoreactive for one of the four interneuronal markers. The majority (16/21) of the immunoreactive interneurons were PV^+ and vasoactive intestinal polypeptide- or CR-negative. Because PV^+ cells do not co-localize somatostatin or cholecystokinin (McDonald and Mascagni, 2002; Mascagni and McDonald, 2003), no additional staining was performed on the PV^+ interneurons. PV^+ immunostaining was usually confined to the soma but occasionally spread to proximal dendrites. Examination of the combined electrophysiological and immunohistochemical data revealed that half (8/16) of the PV^+ interneurons were BF interneurons [making up 61% (8/13) of the total BF subpopulation (Fig. 2A)], and the other half (8/16) were SF interneurons [making up 57% (8/14) of the total SF subpopulation (Fig. 2B)]. No RF or FF interneurons were PV^+. Among the five remaining

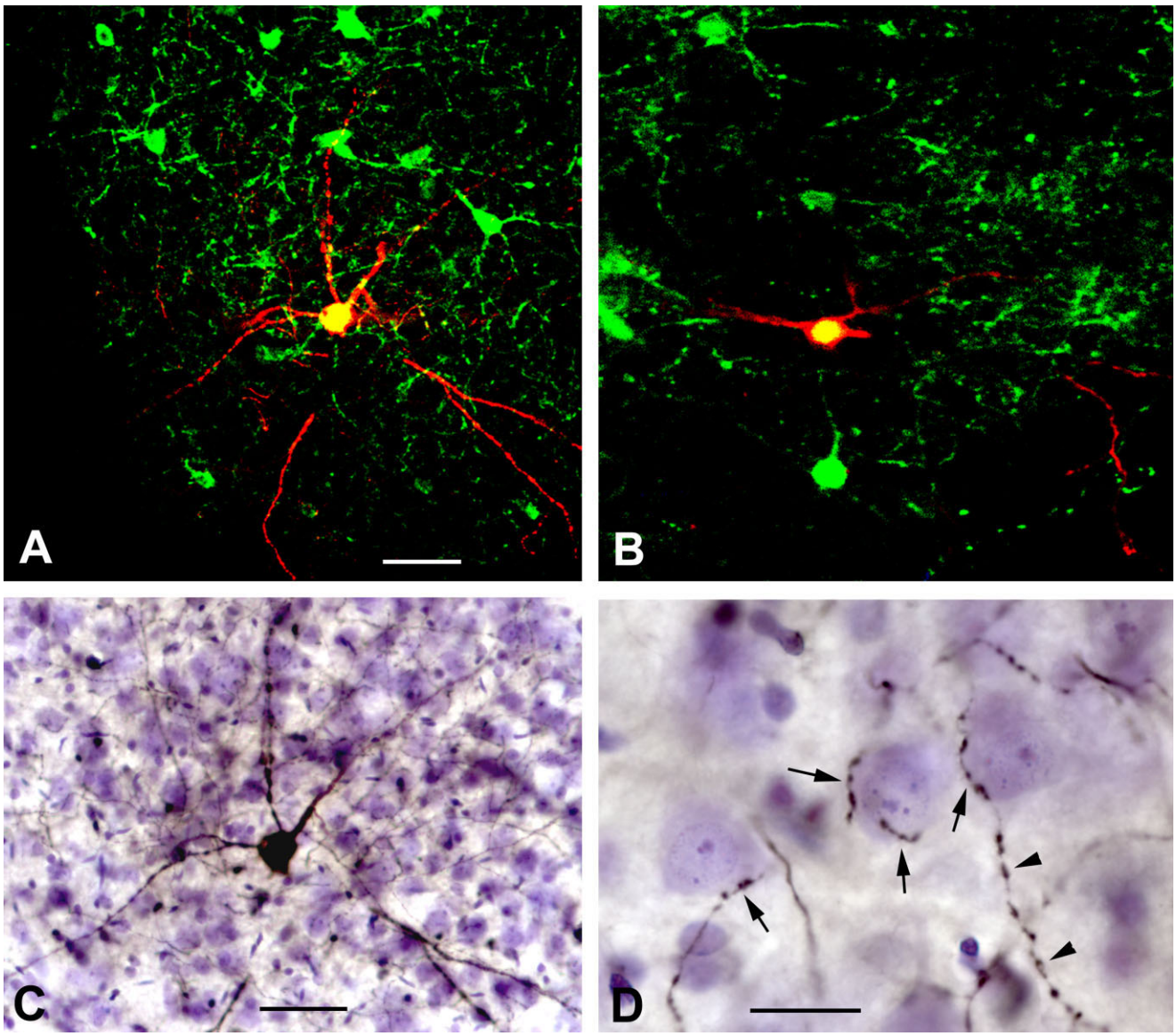

Fig. 2. Burst-firing and stutter-firing interneurons express the calcium-binding protein parvalbumin. **A:** Merged confocal image of the biocytin-filled PV^+ burst-firing interneuron. Biocytin is red. PV^+ neurons are labeled green. Yellow indicates double labeling (i.e., biocytin-filled structures that are PV^+). The cell body and portions of the primary dendrites of this interneuron are PV^+. **B:** Merged confocal image of the PV^+ stutter-firing interneuron. Biocytin is red. PV^+ neurons are labeled green. The cell body of this interneuron is PV^+ (yellow). **C:** Digital photomicrograph of the PV^+ neuron shown in A after visualization for light microscopy with ABC histochemistry and counterstaining with cresyl violet. **D:** Photomontage of a cresyl-violet-stained section, showing a portion of the axonal arborization of the neuron shown in C. Its biocytin-filled axonal collaterals (black) form multiple contacts with the somata of three presumptive pyramidal neurons (arrows). The cell on the right receives additional contacts along the proximal portion of a downwardly projecting process, presumed to be a dendrite (upper arrowhead); this axon then continues its downward course, forming a series of varicosities (lower arrowhead) that do not contact cresyl-violet-stained structures. Scale bars = 50 μm in A (applies to A,B); 50 μm in C; 20 μm in D.

immunopositive interneurons that were not PV^+, two were immunoreactive for CR, two were immunoreactive for somatostatin, and one was immunoreactive for cholecystokinin. The two CR^+ interneurons and the one cholecystokinin$^+$ interneuron showed properties similar to those of the RF subpopulation of interneurons, whereas the two somatostatin$^+$ interneurons more closely resembled the FF subtype. The results of this study are summarized in Table 1. As noted, 57% of the biocytin-filled

TABLE 1. Summary of Results[1]

	Electrophysiological subtypes			
Immunolabel	BF	SF	RF	FF
PV (+/total)	8/13	8/14	0/11	0/10
CR/VIP	0/13	0/14	2/11	0/10
SOM	0/13	0/14	0/11	2/10
CCK	0/13	0/14	1/11	0/10
No signal	5/13	6/14	8/11	8/10

[1]BF, burst-firing; SF, stutter-firing; RF, regular-firing; FF, fast-firing; PV, parvalbumin; +, immunopositive; total, total number of recovered biocytin-filled cells; CR, calretinin; VIP, vasoactive intestinal peptide; SOM, somatostatin; CCK, cholecystokinin.

TABLE 2. Physiological Properties of PV-Positive BF and SF Interneurons[1]

	Vm	Rm	Half-spike width[2]	10-90% Rise rime	Firing pattern		I_h		
	(mV)	(MΩ)	(msec)	(msec)	Slow-regular	Fast-stuttering	Slow[3]	Fast[4]	No
BF (PV^+)	−61 ± 1.0 (7)	145 ± 6.2 (7)	0.73 ± 0.12 (7)	0.43 ± 0.07 (7)	88% (7/8)	12% (1/8)	14% (1/7)	86% (6/7)	—
SF (PV^+)	−60 ± 0.3 (7)	141 ± 2.8 (7)	0.62 ± 0.03 (7)	0.38 ± 0.01 (7)	—	100% (8/8)	71% (5/7)	—	29% (2/7)
RF	−60 ± 1.8 (11)	449 ± 68 (11)	1.17 ± 0.05 (11)	0.51 ± 0.02 (11)	100% (11)	—	18% (2/11)	82% (9/11)	—
FF	−60 ± 2.1 (10)	138 ± 19 (10)	0.67 ± 0.05 (6)	0.32 ± 0.02 (6)	—	—	20% (2/10)	—	80% (8/10)

[1]Vm, resting membrane potential; Rm, membrane input resistance; BF, burst-firing; SF, stutter-firing; RF, regular-firing; FF, fast-firing. Note that the one PV^+ BF cell that is classified as fast-stuttering had such a high rate of spontaneous bursts of action potentials that is was impossible to obtain a clear picture of its true firing pattern. The mixed effect was a pattern that looked like a fast-stuttering response. [2]Measured at half-peak amplitude. [3]Time constant >100 msec. [4]Time constant <100 msec.
Note: The 1 PV+ BF cell that is classified as "fast-stuttering" had such a high rate of spontaneous bursts of action potentials that is was impossible to obtain a clear picture of it's true firing pattern. The mixed effect was a pattern that looked like a fast-stuttering response.

neurons showed no immunoreactivity for any of the cytosolic markers tested. We have previously demonstrated that subpopulations of PV-, CR/vasoactive intestinal polypeptide-, somatostatin-, and cholecystokinin-positive interneurons collectively constitute virtually the entire population of BLA interneurons (Mascagni and McDonald, 2003). Consequently, the lack of immunoreactivity in 57% of filled cells would appear mainly to represent false-negatives resulting from elution of the antigen into the patch pipette during recording, suggesting that fill times shorter than 15 minutes may be necessary to maintain immunogenicity (Kawaguchi, 1995).

Physiological and anatomical characterization of BF and SF PV interneurons

The data above indicate that PV^+ interneurons represent a functionally diverse subpopulation of BLA interneurons, comprising both BF and SF interneurons. Here, we expand on this observation by comparing the physiological properties of PV^+ BF and SF interneurons. No significant difference was observed in the Rm for the PV^+ BF and SF subpopulations compared with the grouped data for each subpopulation ($P > 0.5$ for both groups), suggesting that the PV^+ interneurons were not distinct subpopulations of BF and SF interneurons. Hence, the physiological properties of PV^+ BF and SF interneurons are summarized in Table 2 and are compared with those of RF and FF interneurons.

As illustrated in Table 2, BF and SF PV^+ interneurons share several basic physiological properties. For example, the resting membrane potential (Vm; $P > 0.5$), the membrane input resistance (Rm; $P = 0.38$), and the properties of single action potentials are similar in each subgroup. However, compared with typical BLA projection neurons, for example (Rm = 58 ± 2 MΩ; 10–90% rise time = 0.88 ± 0.01 msec; half-spike width = 1.1 ± 0.01 msec; n = 7), both BF and SF PV^+ interneurons had a significantly higher Rm ($P < 0.001$), a faster action potential rise time ($P < 0.0002$), and shorter half-width ($P < 0.0001$). These data suggest that the input–output relationship for BLA projection neurons and PV^+ interneurons will differ markedly in response to afferent input.

However, as noted above, despite sharing a cytochemical phenotype and several intrinsic membrane properties, BF and SF PV^+ interneurons express distinct physiological properties. For example, one of the defining features of BF interneurons was presence of spontaneous bursts of action potentials in baseline recordings (Fig. 1C), which in voltage clamp mode were seen to be driven by rapidly summating high-frequency excitatory postsynaptic currents (EPSCs; Fig. 3A, upper trace, arrow). In contrast, bursts of summating EPSCs were never observed in any SF interneuron (Fig. 3A, lower trace). Similarly, even though the input resistances of BF and SF PV^+ interneurons are almost identical, BF interneurons showed a more pronounced activation of I_h channels in response to hyperpolarizing current injection than did SF interneurons, as reflected by the more marked depolarizing sag in the voltage response of BF interneurons (Fig. 3B). A comparison of the rate of onset of the depolarizing sag in response to a standardized 250-pA hyperpolarizing current step revealed two distinct time constants for activation. Not only was the potential change mediated by I_h more pronounced in BF interneurons but the rate of onset (τ) was significantly faster ($\tau = 61 \pm 16$ msec, n = 7, $P = 0.03$) compared with that observed in SF interneurons ($\tau = 248 \pm 75$ msec, n = 5). Moreover, 29% of SF interneurons showed no I_h-mediated depolarizing sag, suggesting a differential expression of I_h channel(s) in subpopulations of PV^+ interneurons. A typical response of a PV^+ BF and SF interneuron to application of the I_h channel blocker ZD7288 (30 μM) is illustrated in Figure 3C. Application of ZD7288 abolished the depolarizing sag seen in all BF neuron tested (n = 4), caused an ~6.0- ± 3.1-mV hyperpolarizing shift in the membrane potential, and significantly increased the Rm from 101 ± 12 MΩ to 167 ± 16 MΩ ($P < 0.05$). In contrast, ZD7288 had no significant effect on either the membrane potential or the Rm of PV^+ SF neurons.

Moreover, PV^+ BF and SF interneurons showed a differential response to depolarizing current injection. A representative example of the typical firing pattern for BF and SF PV^+ interneurons is illustrated in Figure 4A. Thus, BF interneurons fired at frequencies of up to 100 Hz within the first 200 msec after the onset of the depolarizing current injection and then settled into a modal firing rate of ~20 Hz for the remainder on the current pulse (Fig. 4A, left trace). In contrast, SF interneurons stutter-fired at 100 ± 19 Hz (range 5–200 Hz, n = 7) in segments ranging from 20 to 400 msec in duration. The pattern of stutter-firing also differed from neuron to neuron, as shown in Figure 4A (right trace). Hence, some SF interneurons only stutter-fired at the beginning of the depolarizing current injection, whereas others fired a short segment at the beginning of the pulse and then fired another longer segment at the end of the current pulse (see Fig. 6A, inset). Similar stutter-firing patterns have been re-

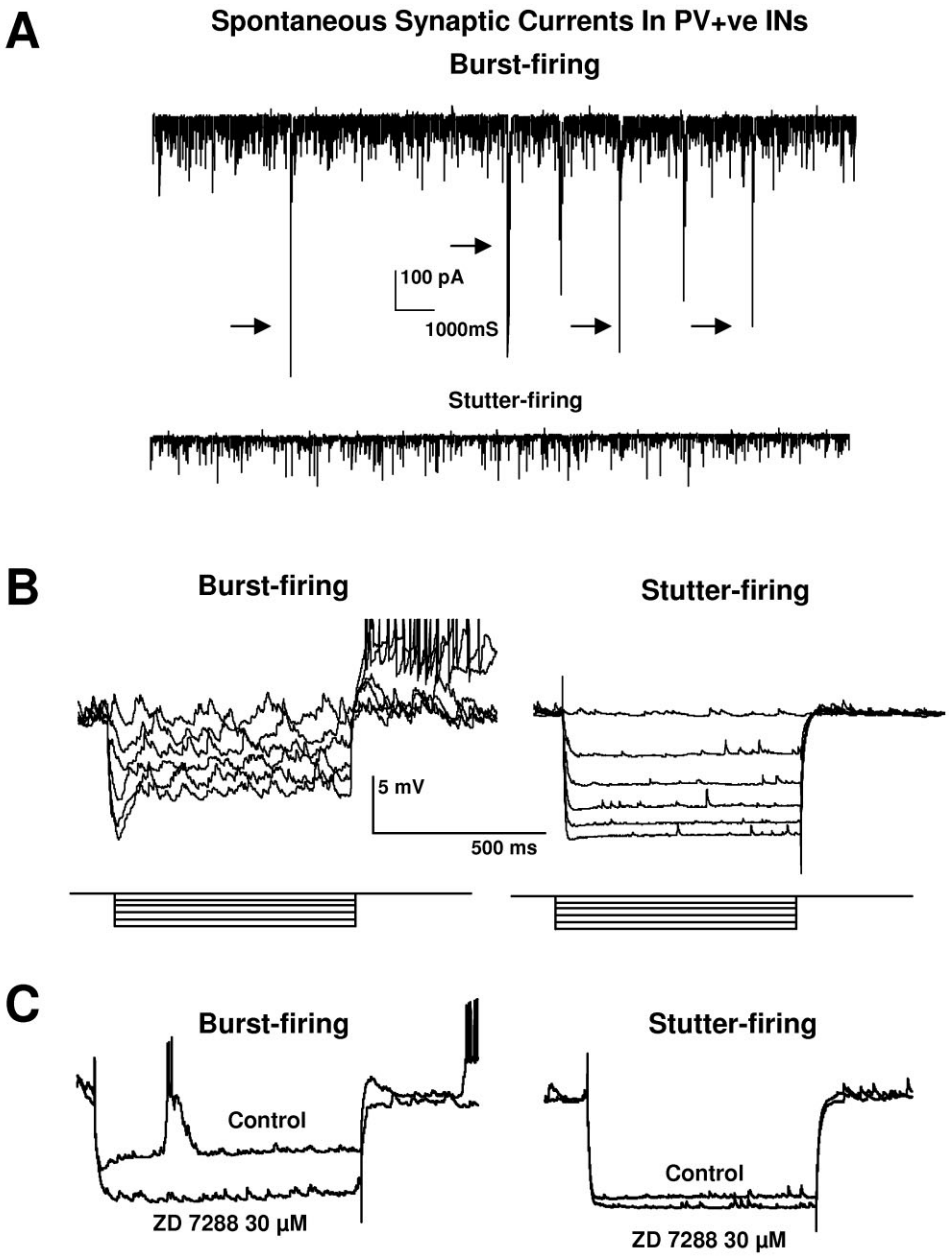

Fig. 3. Local network connections and intrinsic membrane properties differentiate two subtypes of parvalbumin-containing interneurons in the BLA. **A:** Typical 18-second segment of continuous voltage clamp recordings showing the occurrence of rhythmic bursts of compound EPSCs (arrows) in a PV^+ burst-firing interneuron (upper trace) but not in the spontaneous synaptic activity seen in a PV^+ stutter-firing interneuron (lower trace). In both traces, small downward deflections are monosynaptic EPSCs. Holding potential = −60 mV. **B:** The voltage response (upper trace) of burst- and stutter-firing interneurons to hyperpolarizing current injection of increasing amplitude (lower trace, 50–250 pA). Note the pronounced depolarizing "sag" in the voltage response of the burst-firing interneuron, which was absent in the stutter-firing interneuron. **C:** The voltage response (upper trace) of burst- and stutter-firing interneurons to hyperpolarizing current injection before and during application of the specific I_h channel blocker ZD7288 (30 μM).

ported in a subpopulation of PV^+ interneurons in the neocortex (Kawaguchi and Kubota, 1997; Markram et al., 2004).

SF interneurons also showed a high level of voltage rectification in response to depolarizing current injection, which may contribute to their distinctive firing pattern. Hence, for PV^+ BF interneurons, a plot of the steady-state voltage deflection as a function of the amplitude of depolarizing current injection showed a linear current–voltage relationship (Fig. 4B, squares). In contrast, the current–voltage relationship for PV^+ SF interneurons was curvilinear (Fig. 4B, asterisks), with an asymptote close to the threshold for action potential generation (approximately −50 mV). Thus, the extent to which transient depolarizing

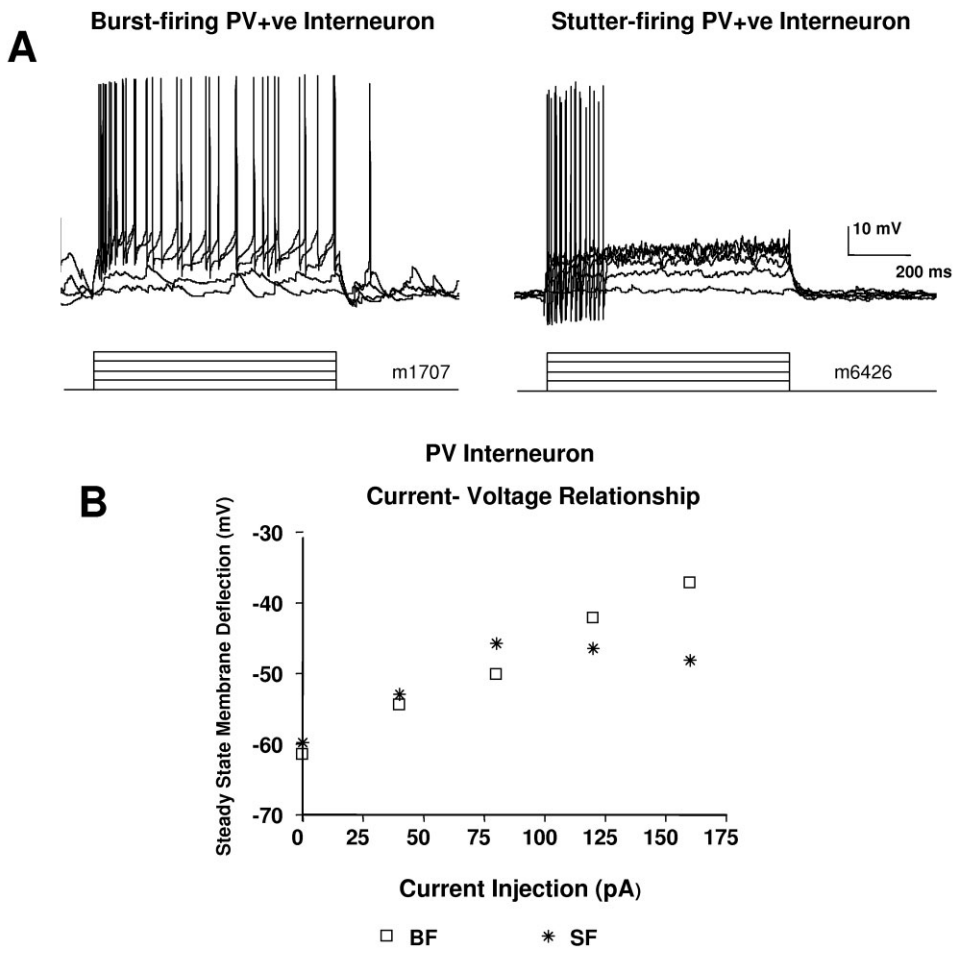

Fig. 4. Firing properties of parvalbumin-containing interneurons. **A:** The voltage response (upper trace) of a PV^+ burst-firing interneuron in response to depolarizing current injection (lower trace, 25–100 pA) compared with that of a PV^+ stutter-firing interneuron. **B:** A plot of steady-state voltage deflection as a function of the amplitude of depolarizing current injection for the two neurons illustrated in A. Burst-firing interneurons show a relatively linear current-voltage relationship (squares). In contrast, the voltage response of stutter-firing interneurons was markedly attenuated with current injection above 75 pA (asterisks).

current injection can overcome the voltage rectification would seem to determine the stutter-firing pattern of SF neurons. Nevertheless, all SF neurons could be made to fire at ~100 Hz throughout the duration of the depolarizing step if the current amplitude was suprathreshold for action potential generation, irrespective of their initial stutter-firing pattern (see Fig. 6A).

To examine the potential mechanisms underlying the difference in voltage-dependent rectification observed in the two PV^+ subgroups, cells were voltage clamped at −60 mV, and a command voltage was applied that was slowly "ramped" from −100 to −40 mV over a 6-second period (Fig. 5, upper trace). At command potentials more negative than −60 mV (dashed line), BF and SF PV^+ interneurons showed a similar current–voltage relationship (BF, middle trace; SF, bottom trace). However, at command potentials more positive than −60 mV, the current response of SF interneurons showed a marked outward rectification (Fig. 5, arrow) compared with BF interneurons.

BF PV^+ interneurons also fired a relatively consistent number of action potentials in response to depolarizing current injection that was suprathreshold for action potential generation (Fig. 6A), a firing pattern that was mimicked during spontaneous bursts of action potentials (Fig. 6A, inset). In contrast, the number of action potentials generated in SF PV^+ interneurons tended to correlate positively with the amplitude of the suprathreshold current injection. Hence, a plot of action potential number as a function of suprathreshold current injection (Fig. 6B) showed no correlation between current injection and spike number in BF interneurons. Although there was a trend toward a positive correlation between spike number and current amplitude in SF, this did not reach the threshold for significance.

Previously, we have shown that the firing properties of BLA projection neurons are regulated by the relative expression of an afterhyperpolarizing potential (AHP) that follows single spikes or trains of spikes (Asprodini et al., 1992). An analysis of AHPs in PV^+ interneurons revealed two additional contrasting properties of PV^+ BF and SF interneurons. Hence, when measured close to the threshold for action potential generation (−50 mV), the amplitude of the AHP following a single action potential in BF

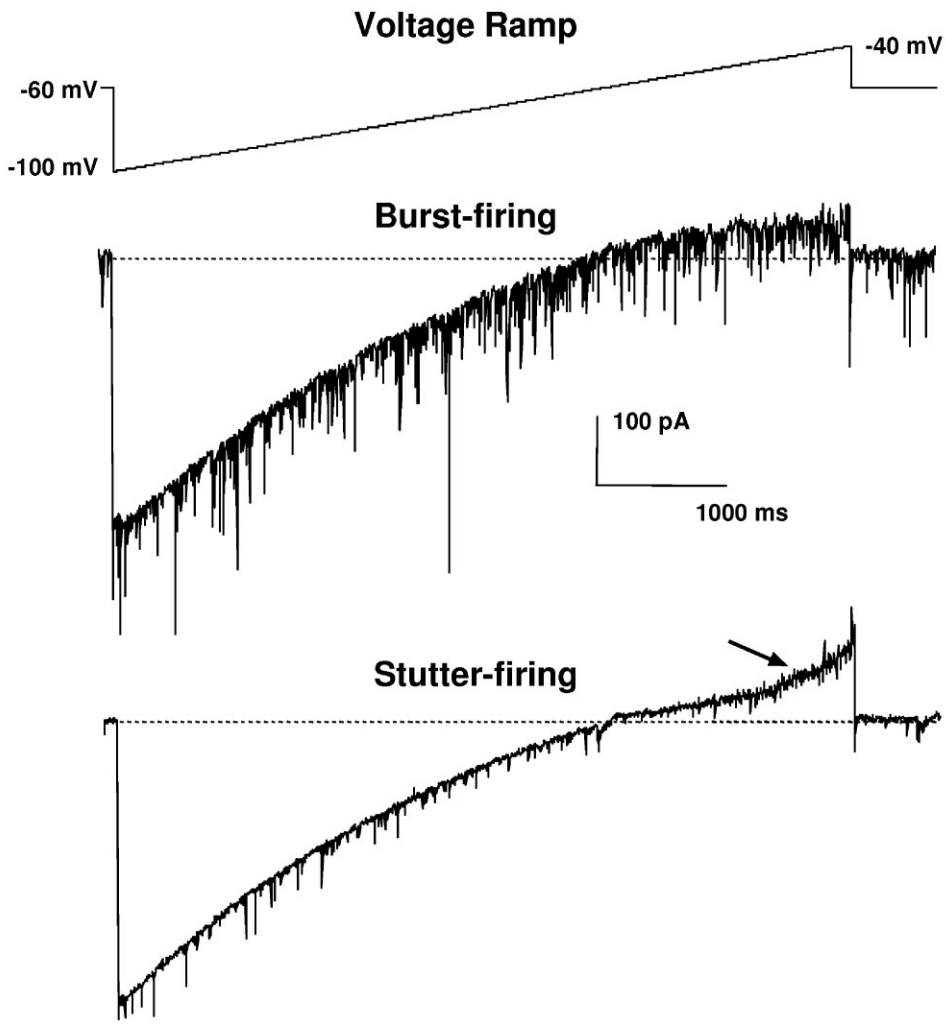

Fig. 5. Differential expression of an outwardly rectifying current by stutter-firing parvalbumin-containing interneurons. A plot of the steady-state current generated in response to a voltage ramp of −100 to −40 mV (upper trace) in burst-firing (middle trace) and stutter-firing (lower trace) interneurons revealed the presence of a pronounced outward rectification (arrowed) in the current response of PV^+ stutter-firing interneurons.

interneurons was significantly smaller (12 ± 1.2 mV, n = 7; $P = 0.02$), but the duration was longer (14 ± 2.3 msec, n = 7; $P = 0.01$) compared with that observed in SF interneurons (AHP amplitude, 17 ± 1.1 mV; AHP duration, 6.1 ± 1.2 msec, n = 7). These data suggest that differences in the firing patterns of the two subpopulations of PV^+ interneurons could be determined, in part, by the differential expression of those ion channels mediating the amplitude and duration of the postspike AHP.

The reverse pattern was seen in the expression of the slow AHP following a train of action potentials elicited close to the resting membrane potential (−60 mV). Here, little or no slow AHP is observed in PV^+ BF interneurons following a train of action potentials (Fig. 7A, left trace), with no correlation between the number of spikes elicited during the train and either the amplitude (Pearson correlation coefficient: r = −0.15, $P = 0.47$, n = 7; Fig. 7B, left trace) or duration (Pearson r = 0.30, $P = 0.18$; Fig. 7C, left trace) of the slow AHP. It is interesting that PV^+ SF interneurons showed a robust slow AHP, the amplitude of which showed a significant and positive correlation with the number of spikes in the preceding train (Pearson r = −0. 80, $P = 0.01$, n = 7; Fig. 7B, right trace) and with AHP duration (Pearson r = 0.59, $P = 0.006$; Fig. 7C, right trace).

Finally, we examined whether differences in the morphology of PV^+ interneurons may correlate with the observed difference in physiological properties. However, no difference was observed in the morphology of the two subtypes of PV^+ interneuron. Both types of PV^+ interneurons exhibited ovoid or multipolar somata and four or five sparsely branched, spine-sparse dendrites that were sometimes beaded (Figs. 2, 8, 9). The lengths and widths of somata of PV^+ BF interneurons (20.9 ± 4.8 μm and 15.9 ± 3.8 μm, respectively; mean ± SD) were not significantly different from those of PV^+ SF interneurons (20.6 ± 5.3 μm and 17.8 ± 4.8 μm, respectively; $P > 0.05$). The axonal arborizations of PV^+ interneurons were 300–

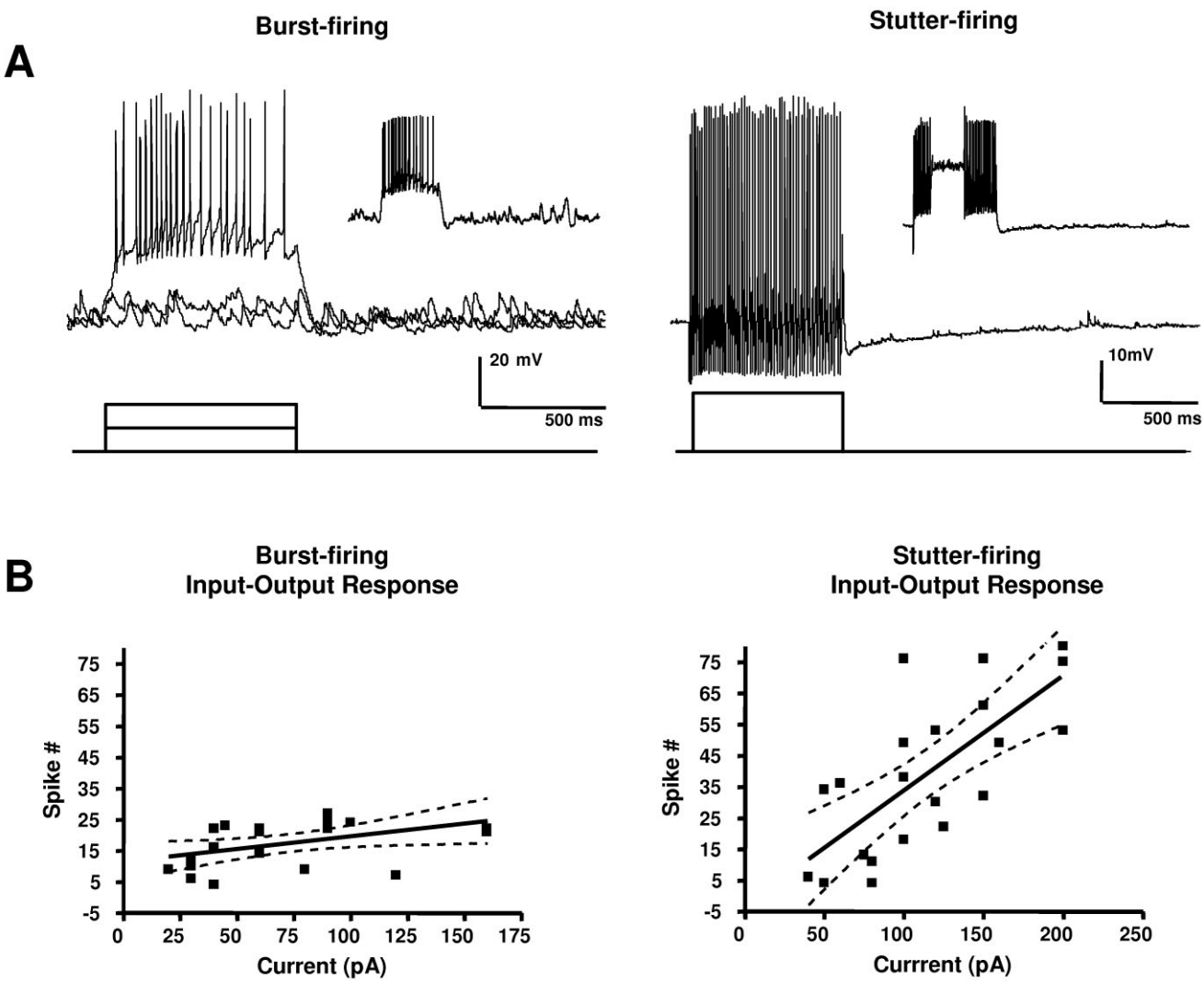

Fig. 6. A comparison of the input–output relationship of burst-firing and stutter-firing interneurons. **A:** In response to depolarizing current injection of increasing amplitude (lower trace), PV^+ burst-firing interneurons fired a relatively consistent number of action potentials (upper left trace). In the same neuron, bursts of spontaneous excitatory synaptic activity evoked a similar firing frequency (inset left). In contrast, stutter-firing PV^+ interneurons (inset right) fired bursts of action potentials whose number positively correlated as a function of stimulus intensity. **B:** A scatterplot of the input-output response of PV^+ interneurons. Spike number is plotted as a function of depolarizing current injection for all of the neurons in each subgroup. Dashed line in B represents the 95% confidence interval. Note, the stutter-firing pattern could be overcome with suprathreshold stimulus intensity.

400 μm in diameter in the coronal plane (Figs. 8, 9) and typically extended through most or all of the sections in the 350-μm-thick slices. These axons exhibited numerous axonal varicosities that were 1.0–1.5 μm in diameter (Figs. 2D, 8, 9). Several BF and SF interneurons had well-filled axons that often formed basket-cell-like contacts with somata of presumed pyramidal neurons. Most pyramidal cell somata innervated by axons of PV^+ interneurons received four to six en passant contacts. The PV^+ basket cell with the most intensely stained axon (a BF interneuron) made multiple contacts (4–12 per soma) with 90 Nissl-stained pyramidal cells in three adjacent 75-μm sections (Fig. 2D). Many additional pyramidal-like Nissl-stained somata received fewer contacts (one to three) from this cell. Nevertheless, the majority of axonal varicosities of all biocytin-filled PV^+ interneurons did not appear to contact the somata of Nissl-stained cells (Fig. 2D, arrowheads).

DISCUSSION

In this study, we have used whole-cell patch clamp recording techniques to examine the physiological properties of 48 visually identified putative interneurons from the rat BLA. Here we report that BLA interneurons can be differentiated into four electrophysiologically distinct subtypes based on their intrinsic membrane properties and their response to afferent synaptic input. Interneuron subtypes were named according to their characteristic firing pattern generated in response to transient depolarizing

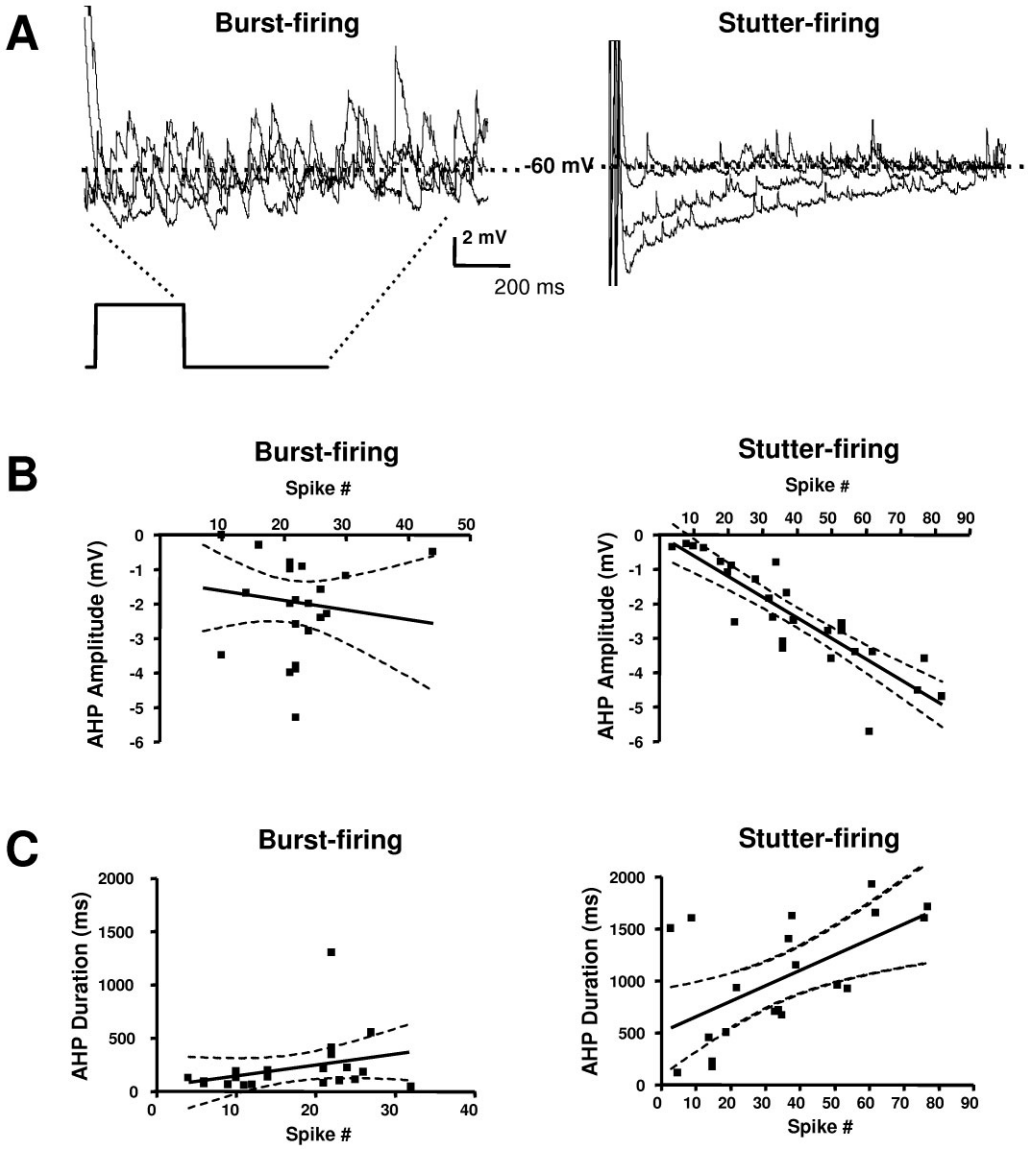

Fig. 7. Differential expression of a slow afterhyperpolarizing potential (AHP) in burst-firing and stutter-firing interneurons. **A:** A representative illustration of the afterhyperpolarizing potentials observed in response to a train of action potentials in burst-firing (right trace) and stutter-firing (left trace) interneurons. **B:** A plot of AHP amplitude as a function of spike number for all neurons in each subgroup. **C:** A plot of the AHP duration as a function of spike number in the same neurons illustrated in B. Dashed lines in B and C represent the 95% confidence interval for the correlation coefficients.

current injection and were grouped as follows: 1) burst-firing interneurons (n = 13), 2) regular-firing interneurons (n = 11), 3) fast-firing interneurons (n = 10), and 4) stutter-firing interneurons (n = 14). Post hoc histochemical visualization confirmed that all 48 recorded neurons had morphological properties consistent with their being nonpyramidal interneurons. Moreover, by using triple immunofluorescence for calcium-binding proteins in conjunction with patch clamp recording, we further demonstrate that over 60% of BF and SF interneurons also expressed the calcium-binding protein PV. These data extend our earlier studies (McDonald and Mascagni, 2001a; Muller et al., 2003) and demonstrate that interneurons of the BLA show both physiological and neurochemical diversity. Moreover, we demonstrate that the burst- and stutter-firing patterns positively correlate with PV^+ immunoreactivity, suggesting that these neurons may represent functionally distinct subpopulations. This is also the first study to visualize the axonal arborizations of *individual* PV^+ interneurons. Many axonal collaterals of both burst-firing and stutter-firing PV^+ interneurons made multiple basket-cell-like contacts with somata of presumptive pyramidal cells.

Categorization of interneuron subpopulations

We believe that the results from the present study offer compelling evidence that morphologically identified BLA

Fig. 8. Morphological reconstruction of the burst-firing PV^+ neuron shown in Figure 3A,C,D. Only the dendrites and axonal branches in the 75-μm-thick section containing the cell body are drawn. Additional axonal branches extended into two adjacent 75-μm-thick sections. **Inset** shows the location of this interneuron in the BLA (bregma −2.0). Only the cell body and dendrites are drawn in the inset; the field containing the axonal arborization is show in gray. Note that the thick process extending into dorsal portions of the BLA is not a dendrite but one of the main branches of the axon. The axon of this cell contacted the somata of over 100 surrounding Nissl-stained cells. Lat, lateral nucleus. Scale bar = 100 μm.

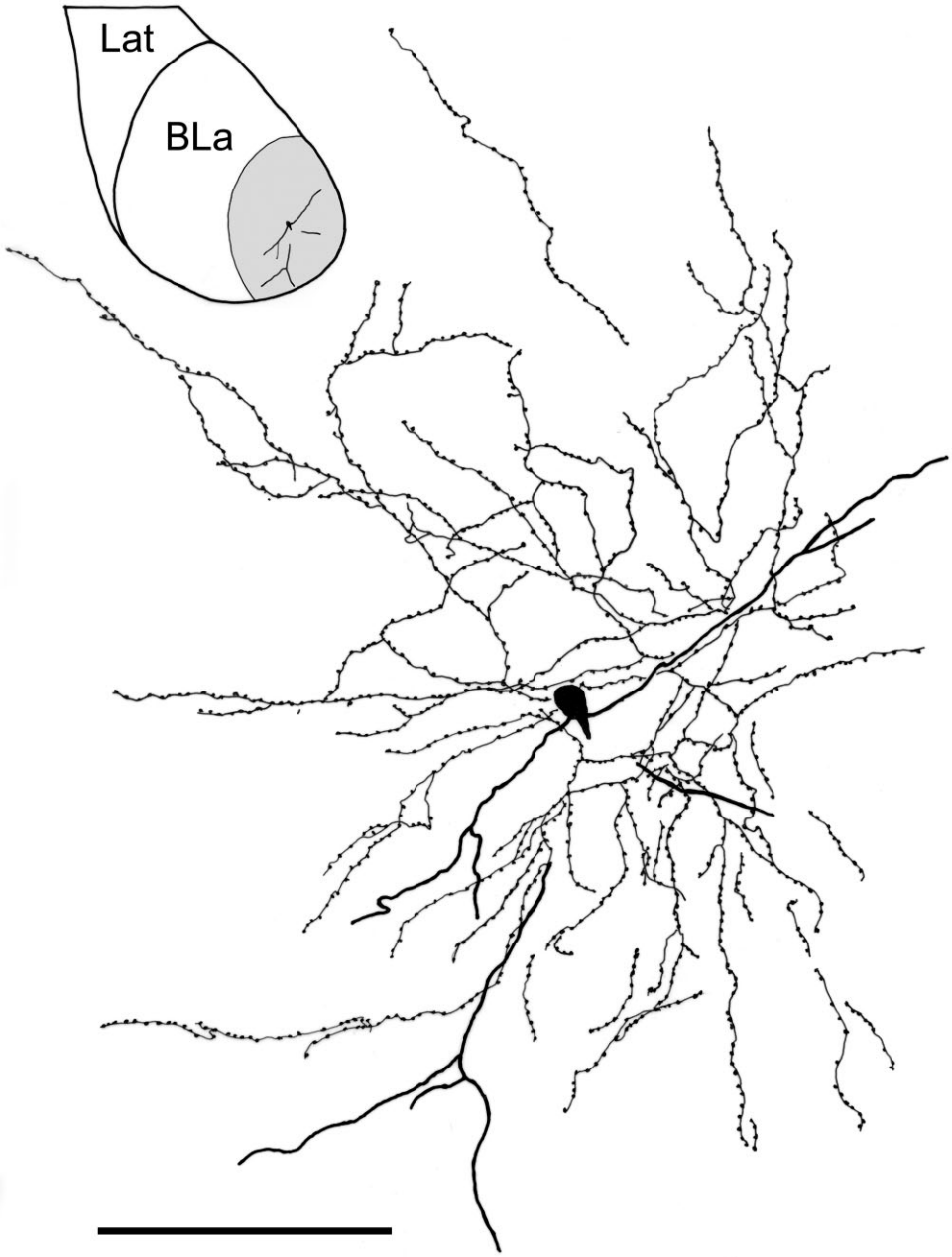

Fig. 9. Morphological reconstruction of a stutter-firing PV^+ interneuron. Only the dendrites and axonal branches in the 75-μm-thick section containing the cell body are drawn. Additional axonal branches extended into three adjacent 75-μm-thick sections. **Inset** shows the location of this interneuron in the BLA (bregma −2.2). Only the cell body and dendrites are drawn in the inset; the field containing the axonal arborization is show in gray. The axon of this cell contacted the somata of 17 surrounding pyramidal cells in this section. Lat, lateral nucleus. Scale bar = 100 μm.

interneurons can be differentiated into at least four distinct physiological subtypes. Physiological diversity of interneuron subpopulations is not without precedence in the CNS. For example, three or more physiologically distinct subpopulations of interneurons have been identified in the frontal cortex (Kawaguchi and Kubota, 1997), sensorymotor cortex (Gupta et al., 2000), hippocampus (Pawelzik et al., 2002), and neostriatum (Kawaguchi, 1993). In each case, the primary criteria by which these interneurons were differentiated was their firing pattern, generated in response to transient depolarizing current injection. There is, however, some discussion about the relative merits of taxonomy when examining the function of cortical interneurons (Parra et al., 1998; McBain and Fisahn, 2001; Nelson, 2002). For instance, for the hippocampus, Parra and colleagues (1998) identified 16 distinct morphological phenotypes of interneuron, with 25 different combinations of response to four receptor agonists, suggesting

that hippocampal interneurons cannot be easily categorized into distinct subpopulations. Nonetheless, despite the potential complexity of this categorization, only three modes of action potential discharge were identified, suggesting that subgroups of interneurons throughout the cerebrum may exhibit canonical properties, over which a mosaic of additional morphological, pharmacological, and physiological properties is superimposed, shaping the functional response of individual interneurons. Consistently with this hypothesis, a recent correlative mapping study of neocortical interneurons, in which the mRNA profiles for 26 ion channels and three calcium-binding proteins were correlated with the expression of 61 physiological properties, revealed differential clustering of ion channels around the three calcium-binding proteins, the PV cluster, the CB cluster, and the CR cluster (Toledo-Rodriguez et al., 2004). Consequently, we believe that our dual approach of first identifying the discharge properties of BLA interneurons and then correlating this with their calcium-binding protein expression pattern might be the most effective way to determine the basic elements of the BLA microcircuitry.

Physiological diversity in BLA interneurons

The BLA has been described as a cortex-like structure (Carlsen and Heimer, 1988), with BLA interneurons showing a morphological, anatomical, and neurochemical profile remarkably similar to that found in the neocortex (Kemppainen and Pitkänen, 2000; McDonald and Betette, 2001; Pitkänen and Kemppainen, 2002; Muller et al., 2003). For the purposes of this discussion, we will compare and contrast our results with those obtained from interneuron subpopulations in the neocortex. There is extensive evidence in the cortical literature that the electrophysiological properties we have examined are dependent on the activation of specific ion channels (Llinas, 1988; Rudy, 1988; Rudy and McBain, 2001). Much less is known about these relationships in the BLA. However, we believe that the incredible similarity between cortical and BLA interneurons validates the use of cortical data to infer which ion channels may be involved in similar properties seen in BLA interneurons.

As might be predicted, a considerable degree of overlap exists in the discharge profiles observed in the four subtypes of BLA interneuron and those found in cortical areas. Perhaps the most common subclass of interneurons observed outside the BLA is the FS neurons. First described in the neocortex (McCormick et al., 1985; Connors and Gutnik, 1990), the properties of these neurons have become the prototypical definition of "interneurons" in many electrophysiological studies throughout the brain. However, the "fast-spiking" classification may be somewhat misleading in that the FS nomenclature originally referred to the spike duration and not necessarily to the discharge pattern. Moreover, FS neurons are often reported to show an abrupt episode of repetitive discharges (Kawaguchi, 1995; Markram et al., 2004) in response to depolarizing current injection. A review of the literature suggests that many reported examples of FS neurons show some form of abrupt discharge pattern, as do approximately 30% of BLA interneurons. Markram and coworkers have more accurately termed interneurons with this firing pattern as stuttering (Gupta et al., 2000; Markram et al., 2004). Hence, our SF interneurons most probably correlate with the FS subtype of interneuron seen in other brain regions. Consistent with this hypothesis, FS interneurons of the neocortex and hippocampus, as with BLA SF interneurons (see below), contain PV and form basket-like connections with the somata of glutamatergic projection neurons (Kawaguchi and Kubota, 1993; Wang et al., 2002; Pawelzik et al., 2002). Significantly, the neocortical "PV gene cluster" observed by Markram and colleagues (Toledo-Rodriguez et al., 2004) contained mRNA expression profiles for Kv3.1 and Kv3.2, HCN1 and HCN2, as well as several members of the Kv1 family, including Kv1.1.

Voltage-gated K^+-channel (Kv) subunits Kv3.1 and Kv3.2 allow the fast repolarization of action potentials and, hence, are thought to be a major determinant of the FS phenotype (McBain and Fisahn, 2001; Rudy and McBain, 2001). The fast spike duration of SF BLA interneurons (~0.6 msec) is similar to that observed in FS neurons and suggests that these neurons might also express K^+ channels containing the Kv3.1 and/or Kv3.2 subunits. Moreover, Markram and colleagues reported that dendrotoxin K (DtxK), a blocker of channels containing Kv1.1 subunits, abolished stutter-firing in neocortical interneurons, suggesting that SF interneurons in the BLA may also express the Kv1.1 subunit. Members of the Kv1 family also give rise to a 4-AP-sensitive delayed rectifying current (Coetzee et al., 1999; Wang et al., 2002). One of the defining features of SF interneurons in the BLA was the marked outward rectification seen in their current–voltage relationship at membrane potentials more positive than −50 mV (Fig. 5), further suggesting that these interneurons resemble FS neurons and most probably express K^+ channels containing Kv1.2 and/or Kv1.6 subunits that are know to contribute to outward rectification (Coetzee et al., 1999).

The family of hyperpolarization-activated cyclic nucleotide-gated nonselective cation (HCN) channels, which mediate the expression of I_h, displays markedly different activation kinetics (Ludwig et al., 1998; Santoro et al., 2000). Hence, HCN1 channels activate rapidly on hyperpolarization (tens of milliseconds), HCN2 channels activate more slowly (hundreds of msec), and HCN4 activate the slowest of all HCN channels (seconds; Ludwig et al., 1998; Santoro et al., 2000). A characteristic of SF interneurons is that they showed little I_h activation with membrane hyperpolarization and what was present at −80 mV activated slowly (248 msec), suggesting that this subpopulation of PV^+ interneurons may preferentially express HCN2 channels. In contrast, BF PV^+ interneurons were differentiated from SF PV^+ neurons not only by their discharge pattern but also by their rapid rate of activation of I_h (~60 msec). An I_h activation rate of ~60 msec is close to that reported for HNC1 channels. Intriguingly, the neocortical "PV gene cluster" included both the HCN1 and HCN2 genes.

Results from the present study suggest that more than one PV^+ cell type may contribute to the "PV gene clusters." Consistently with this hypothesis, BF PV^+ chandelier cells (Buhl et al., 1994b) and multipolar bursting (MB) interneurons (Blatow et al., 2003) have been identified. As with BF interneurons of the BLA, the firing pattern of these neurons was also characterized by an initial burst of action potentials, followed by a subsequent train of rhythmic, low-frequency action potentials. In the neocortex, PV^+ and CB^+ interneurons are regarded as nominally nonoverlapping cell populations (Kawaguchi and Kubota,

1997). It is noteworthy, therefore, that all PV^+ MB neurons coexpress CB. In the BLA, ~80% of PV^+ interneurons contain CB (McDonald and Betette, 2001), suggesting that PV^+ BF interneurons may serve the same functional role as cortical chandelier cells and MB neurons.

Interneurons with properties similar to regular-firing BLA interneurons are also found throughout the brain and have been alternately labeled regular-spiking (Cauli et al., 1997; Kawaguchi and Kubota, 1997, 1998) or nonaccommodating interneurons (Gupta et al., 2000). In the hippocampus and neocortex, regular-spiking interneurons contain the neuropeptide cholecystokinin and show a maximal firing rate of ~50 Hz (Kawaguchi and Kubota, 1998; Pawelzik et al., 2002), which is similar to the maximal firing rate observed in our RF neuron (~20 Hz). Cholecystokinin$^+$ interneurons constitute approximately 25% of the total interneuron population of the BLA (Mascagni and McDonald, 2003) and fall into two morphological subtypes: 1) type L neurons characterized by their large somata and thick dendrites and 2) type S neurons characterized by their small somata and thin dendrites (Mascagni and McDonald, 2003). RF neurons have a significantly higher input resistance than any other subpopulation of BLA interneuron, suggesting that these neurons may correspond to the S-type cholecystokinin interneuron. Only one cholecystokinin$^+$ interneuron was recovered in this study, and it remains to be determined whether RF interneurons correspond to either of these two cell types.

Fast-firing interneurons of the BLA were characterized by their ability to fire a nonaccommodating train of action potentials at high frequency throughout the duration of a depolarizing current injection. This property would enable these neurons to follow high-frequency synaptic input with high fidelity. As with SF neurons, the ability of fast-firing interneurons to fire at high frequency most probably results from the expression of one or more members of the Kv3 family of K^+ channel subunits (McBain and Fisahn, 2001; Rudy and McBain, 2001). However, unlike SF neurons, the fast-firing subpopulation of BLA interneurons is unlikely to express K^+ channels containing the Kv1.1 subunit. Intriguingly, a subpopulation of nonaccommodating interneurons in the somatosensory cortex has a similar discharge pattern and coexpresses somatostatin and cholecystokinin but lacks any detectable calcium-binding proteins (Wang et al., 2002). In BLA interneurons, the expression of somatostatin and cholecystokinin is mutually exclusive (McDonald, 1989; McDonald and Mascagni, 2002). Hence, the fast-firing subpopulation of BLA interneurons may correlate with either a somatostatin-expressing subpopulation, or a cholecystokinin subpopulation, or distinct subpopulations of both. The two somatostatin interneurons recovered to date had properties that resembled those of the fast-firing subpopulation of BLA interneurons.

Anatomical characteristics of BLA PV^+ interneurons

The somatodendritic morphology of both BF and SF PV^+ neurons was heterogeneous and resembled that of PV^+ neurons described in previous immunohistochemical studies of the BLA (Kemppainen and Pitkänen, 2000; McDonald and Betette, 2001). However, this is the first study to visualize the axonal arborization of *individual* PV^+ interneurons. The axonal arborization of individual PV^+ neurons was 300–400 μm in diameter, and the somata of presumptive pyramidal cells was a frequent target of axonal varicosities. Axonal collaterals contacting pyramidal cell somata usually formed a series of en passant contacts (usually four to six), similar to that of PV^+ basket cells in the neocortex and hippocampus. Robust PV^+ perisomatic innervation of BLA pyramidal cells has also been observed in previous light and electron microscopic immunohistochemical studies in rats (Kemppainen and Pitkänen, 2000; McDonald and Betette, 2001; Muller et al., 2006), monkeys (Pitkänen and Amaral, 1994), humans (Sorvari et al., 1995), and cats (Smith et al., 1998). Significantly, in the present study, the most axonal varicosities of PV^+ basket cells did *not* contact pyramidal cell somata, suggesting that they may make synaptic contacts with the dendrites and spines of pyramidal neurons (Smith et al., 1998; Muller et al., 2006) or interneurons (Muller et al., 2003, 2005). Likewise, cortical basket cells, including PV^+ basket cells, provide an extensive innervation of distal dendrites and spines in addition to their signature perisomatic innervation of pyramidal cells (Somogyi et al., 1983; Maccaferri et al., 2000).

In a previous light microscopic study of PV^+ neurons, counts revealed that the somata of BLA pyramidal cells are postsynaptic to 50–80 PV^+ axon terminals (unpublished observations by McDonald and Betette, 2001). Insofar as the present study suggests that each individual PV^+ basket cell contributes about four to six axon terminals to pericellular baskets surrounding individual pyramidal cell somata, these data suggest that roughly 10–20 PV^+ basket cells may innervate somata of individual BLA pyramidal cells. Similarly, in the hippocampus, each basket cell forms two to five synapses with each pyramidal cell somata, and it has been estimated that about 25 basket cells innervate cell bodies of individual hippocampal pyramidal cells (Buhl et al., 1994a; Miles et al., 1996).

In the cortex, PV^+ chandelier cells selectively innervate the axon initial segments of cortical pyramidal cells. In the BLA, similar clusters of closely spaced axonal cartridges surrounding the axon initial segments have been observed in Golgi preparations (McDonald, 1982) and in light and electron microscopic immunohistochemical studies (Pitkänen and Amaral, 1994; Sorvari et al., 1996; Muller et al., 2006). Although none of the PV^+ interneurons in the present study appeared to form axonal contacts, it is possible that some of the PV^+ neurons whose axon were not well-filled may belong to this subpopulation of PV^+ interneurons. Alternatively, because BLA chandelier cells have fairly large somata (McDonald and Culberson, 1981; McDonald, 1982), they might not have met the selection criteria we used to preselect putative interneurons visually.

Physiological diversity in PV^+ interneurons

Although PV^+ interneurons of the BLA represent a morphologically heterogeneous subpopulation of BLA interneurons (Pitkänen and Amaral, 1993; McDonald and Betette, 2001), functional diversity has yet to be firmly established. However, results from the present study go some way toward validating the hypothesis that PV^+ interneurons of the BLA can be subdivided into at least two functionally distinct subpopulations.

A defining characteristic of BF PV^+ interneurons is the presence of barrages of high-frequency, summating EPSPs that drive the membrane potential toward threshold

for action potential generation. No other BLA interneuron subpopulation, including the PV^+ SF interneurons, displays similar properties. Spontaneous burst-firing activity was blocked by the addition of glutamate receptor antagonists to the ASCF (not shown), suggesting that this was a response to synchronized synaptic input and did not result from an intrinsic membrane property. In the BLA, PV^+ interneurons receive ~90% of their excitatory afferent input from intrinsic sources (Smith et al., 2000). Recently, we demonstrated that axons collaterals from a single BLA projection neuron can form multiple perisomatic contacts on an individual PV^+ interneuron (McDonald et al., 2005). In contrast, 84% of contacts between hippocampal projection neurons and PV^+ interneurons are reported to be single contacts (Sik et al., 1993). Multiple perisomatic contacts from glutamatergic projection neurons would greatly facilitate the occurrence of spontaneous burst firing in PV^+ interneurons, and it is possible that individual BLA projection neurons make multiple synaptic contacts with BF interneurons but only single contacts with SF interneurons.

In contrast, both BF and SF interneurons make basket-like connections with BLA projections neurons, and each individual PV^+ interneuron can make contacts with a large number of pyramidal projection neurons. These data indicate a high level of reciprocal connectivity between projection neurons and PV^+ interneurons and support the notion that PV^+ interneurons may be critical components in the regulation of synchronized activity in BLA projection neurons. Consistently with this hypothesis, we have shown a significant correlation between the occurrence of rhythmic (~1 Hz) spontaneous IPSPs in BLA projections neurons and the activation of putative interneurons with properties similar to those of BF interneurons (Rainnie, 1999a,b). Hence, PV^+ BF interneurons may act to synchronize the output activity of local ensembles of BLA projection neurons by patterning periods of slow rhythmic inhibition. In contrast, SF interneurons may be responsible for rapid feedback regulation of projection neuron excitability.

The intrinsic membrane properties of BF and SF neurons add further weight to the proposal that the two subpopulations of PV^+ interneurons may act differentially to regulate the output frequency of local ensembles of BLA projection neurons. Unlike SF interneurons, BF interneurons express a prominent depolarizing sag in the voltage response to hyperpolarizing current injection, which was blocked by the nonspecific I_h channel inhibitor ZD7288 (not shown). Activation of I_h channels is often associated with the occurrence of slow intrinsic membrane oscillations in many areas of the CNS, including the BLA (McCormick and Pape, 1990; Pape and Driesang, 1998; Izhikevich, 2001).

Moreover, unlike SF interneurons, BF interneurons cannot maintain trains of high-frequency (100 Hz) action potentials and settle relatively quickly into a slower (~20 Hz) discharge in response to strong excitatory input. The postspike AHP in BF interneurons is smaller in amplitude, but significantly longer in duration (14 msec vs. 6 msec, respectively), than that observed in SF interneurons, suggesting that additional currents may contribute to the AHP in BF neurons. After a single action potential, BLA projection neurons express both a fast and a medium AHP (Rainnie et al., 1993; Faber and Sah, 2002). Whereas the fast AHP was mediated by currents activated during spike repolarization, the medium AHP was mediated by activation of small-conductance calcium-dependent K^+ (SK) channels (Faber and Sah, 2002). It is possible that both BF and SF interneurons express Kv3.1 and Kv3.2 channels that contribute to the expression of the fast AHP (Faber and Sah, 2002) but only BF interneurons express SK channels. Consistent with this hypothesis, we have now demonstrated that PV^+ interneurons of the BLA express high levels of both Kv3.1b and Kv3.2 (McDonald and Mascagni, 2006). Nonetheless, the duration of the AHP seen in BF neurons would ensure that these neurons fire at a slower frequency than SF neurons.

Only SF interneurons showed a slow AHP following periods of repetitive action potential firing. Consequently, although SF neurons may be able to fire at higher frequencies than BF interneurons, the duration of this response may be tightly regulated by the expression of the slow AHP. In BLA projection neurons, the current mediating a similar slow AHP (sI_{AHP}) can be modulated by several neurotransmitters, including corticotropin-releasing factor (Rainnie et al., 1992), glutamate (Rainnie et al., 1994), noradrenaline (Faber and Sah, 2002), and acetylcholine (Washburn and Moises, 1992a; Faber and Sah, 2002). In the hippocampus, each of these neurotransmitters also increases the excitability of local circuit interneurons (Jonas et al., 2004), and one, acetylcholine, can induce rhythmic gamma oscillations at 30–70 Hz in projection neurons that is dependent on activation of interneurons (Traub et al., 1992; Jefferys et al., 1996). Hence, modulation of the slow AHP in SF interneurons of the BLA may function to regulate the expression of gamma frequency oscillations in the BLA.

A defining property of SF interneurons is the presence of a prominent outward rectification at membrane potentials more positive than −60 mV, a property that most probably contributes to the characteristic discharge pattern seen in these neurons. In many areas of the CNS, activation of a muscarine-sensitive, slowly inactivating K^+ current (I_M) contributes to outward rectification observed at potentials close to −60 mV (Halliwell and Adams, 1982; Womble and Moises, 1992). Significantly, dopamine excites a subpopulation of FS interneurons in the prefrontal cortex by attenuating I_M (Gorelova et al., 2002). In the BLA, dopaminergic afferents preferentially target PV^+ interneurons (Asan, 1998; Brinley-Reed and McDonald, 1999), and we and others have shown that dopamine increases that excitability of putative BLA interneurons (Rosenkranz and Grace, 1999; Levita et al., 2003a; Kroner et al., 2005). Hence, dopamine may modulate the excitability of SF interneurons by attenuating the activation of I_M channels. In doing so, dopamine may facilitate the development of fast gamma frequency oscillations in the BLA.

Division of labor within a population of PV^+ neurons is not without precedent. For example, PV^+ interneurons of the hippocampus make up at least three morphologically distinct cell types (McBain and Fisahn, 2001), display two different discharge patterns (Pawelzik et al., 2002), and show differential sensitivity to barbiturates (Pawelzik et al., 1999). In addition, whereas Kv3.1 subunits are ubiquitously expressed in all PV^+ hippocampal interneurons, some show much higher expression levels of Kv3.2 subunits than others (Chow et al., 1999). Potassium channels containing the Kv3.1 and Kv3.2 subunits are differentially modulated by protein kinases (Chow et al., 1999). If a

similar distribution were to occur in BF and SF PV^+ interneurons of the BLA, a single neurotransmitter could evoke markedly different responses in the two subpopulations of neuron.

Functional consequences of PV^+ heterogeneity

Many cognitive processes appear to be dependent on phase-locked oscillations and synchronization. For example, synchronized oscillations in ensembles of reciprocally connected neurons are thought to contribute to selective attention and memory formation, as well as to binding of visual and olfactory information (Rodriguez et al., 1999; Varela et al., 2001; Singer, 2001; Yamaguchi et al., 2004). In the BLA, BF and SF PV^+ interneurons form basket-like contacts around the soma of multiple projection neurons. Perisomatic inhibition is ideally suited to control output by synchronizing the action potential firing of ensembles of projection neurons. Consequently, PV^+ BF and SF interneurons are ideally positioned to regulate synchronous activity in ensembles of BLA projection neurons. Recently, we have demonstrated that PV^+ interneurons of the BLA are interconnected by chemical synapses and dendritic gap junctions into functional networks (Muller et al., 2005). In the neocortex, evidence suggests that networks of electrically and chemically coupled basket cells are necessary to entrain cortical projection neurons at gamma and theta frequency (Tamas et al., 2000; Deans et al., 2001; Hormuzdi et al., 2001). Moreover, Freund (2003) has posited that networks of PV^+ interneurons operate as a "nonplastic, precision clockwork for gamma and theta oscillations, and are indispensable for basic cortical processing." Results from the present study suggest that, in the BLA, two independent networks of PV^+ neurons may exist that could synchronize the output of projection neurons at distinct frequency bands. Hence, a network of BF PV^+ interneurons could synchronize projection neuron ensembles at the slower theta frequency range (4–8 Hz). Whereas networks of SF interneurons may synchronize projection neuron ensembles in the faster gamma range (30–100 Hz). Support for this hypothesis comes from the observation that, in the neocortex, gap junctions are formed exclusively between GABAergic cells of the same class, such as between FS PV^+ cells (Galarreta and Hestrin, 2002; Hestrin and Galarreta, 2005) or between multipolar bursting (MB) PV^+ cells but rarely between MB and FS cells (Blatow et al., 2003).

In the BLA, synchronized oscillations at theta and gamma frequency in local ensembles of projection neurons are thought to mediate the consolidation (Pelletier and Pare, 2004) and recall of fear memory (Seidenbecher et al., 2003), whereas higher frequency (200 Hz) oscillations are associated with the onset of slow-wave sleep (Ponomarenko et al., 2003). In addition, indirect evidence supports a role for PV^+ interneurons in the formation of fear memory. Hence, dopaminergic modulation of interneuron excitability has been shown to facilitate LTP in the lateral nucleus (Bissiere et al., 2003) and cross-modal association in the BLA (Rosenkranz and Grace, 2002). Moreover, the amnestic effect of the nonbenzodiazepine anxiolytic zolpidem in aversive memory tasks is believed to be dependent on the expression of an alpha-1 subunit in $GABA_A$ receptors. In the BLA, PV^+ interneurons are the main interneuron population expressing the alpha-1 subunit (McDonald and Mascagni, 2004). In the hippocampus, zolpidem preferentially enhances the IPSP onto principal neurons originating from fast spiking basket cells compared witho regular spiking basket cells (Thomson et al., 2000), suggesting that subpopulations of PV^+ interneurons may be preferentially activated during fear memory formation. However, it remains to be determined whether distinct subpopulations of PV^+ BLA interneurons contribute to any or all of these behaviors.

ACKNOWLEDGMENTS

The authors thank Dr. John Walsh (CURE/Gastroenteric Biology Center, Antibody/RIA Core, NIH grant DK-41301) for donating the mouse monoclonal antibody to cholecystokinin/gastrin (monoclonal antibody No. 9303). Yerkes National Primate Research Center base grant RR-00165 was awarded by the Animal Resources Program of the NIH.

LITERATURE CITED

Acsady L, Gorcs TJ, Freund TF. 1996. Different populations of vasoactive intestinal polypeptide-immunoreactive interneurons are specialized to control pyramidal cells or interneurons in the hippocampus. Neuroscience 73:317–334.

Aggleton JP. 1992. The amygdala. neurobiological aspects of emotion, memory, and mental dysfunction. New York: Wiley-Liss, Inc.

Aggleton JP. 2000. The amygdala: a functional analysis, 2nd ed. Oxford: Oxford University Press.

Asan E. 1998. The catecholaminergic innervation of the rat amygdala. Adv Anat Embryol Cell Biol 142:1–118.

Asprodini EK, Rainnie DG, Anderson AC, Shinnick-Gallagher P. 1992. In vivo kindling does not alter afterhyperpolarisations (AHPs) following action potential firing in vitro in basolateral amygdala neurons. Brain Res 588:329–334.

Bissiere S, Humeau Y, Luthi A. 2003. Dopamine gates LTP induction in lateral amygdala by suppressing feedforward inhibition. Nat Neurosci 6:587–592.

Blatow M, Rozov A, Katona I, Hormuzdi SG, Meyer AH, Whittington MA, Caputi A, Monyer H. 2003. A novel network of multipolar bursting interneurons generates theta frequency oscillations in neocortex. Neuron 38:805–817.

Brinley-Reed M, McDonald AJ. 1999. Evidence that dopaminergic axons provide a dense innervation of specific neuronal subpopulations in the rat basolateral amygdala. Brain Res 850:127–135.

Buhl EH, Halasy K, Somogyi P. 1994a. Diverse sources of hippocampal unitary inhibitory postsynaptic potentials and the number of synaptic release sites. Nature 368:823–828.

Buhl EH, Han Z-S, Lörinczi Z, Stezhka VV, Karnup SV, Somogyi P. 1994b. Physiological properties of anatomically identified axo-axonic cells in the rat hippocampus. J Neurophysiol 71:1289–1307.

Carlsen J. 1988. Immunocytochemical localization of glutamate decarboxylase in the rat basolateral amygdaloid nucleus, with special reference to GABAergic innervation of amygdalostriatal projection neurons. J Comp Neurol 273:513–526.

Carlsen J, Heimer L. 1988. The basolateral amygdaloid complex as a cortical-like structure. Brain Res 441:377–380.

Cauli B, Audinat E, Lambolez B, Angulo MC, Ropert N, Tsuzuki K, Hestrin S, Rossier J. 1997. Molecular and physiological diversity of cortical nonpyramidal cells. J Neurosci 17:3894–3906.

Chow A, Erisir A, Farb C, Nadal MS, Ozaita A, Lau D, Welker E, Rudy B. 1999. K^+ channel expression distinguishes subpopulations of parvalbumin- and somatostatin-containing neocortical interneurons. J Neurosci 19:9332–9345.

Cobb SR, Buhl EH, Halasy K, Paulsen O, Somogyi P. 1995. Synchronization of neuronal activity in hippocampus by individual GABAergic interneurons. Nature 378:75–78.

Cobb SR, Halasy K, Vida I, Nyiri G, Tamas G, Buhl EH, Somogyi P. 1997. Synaptic effects of identified interneurons innervating both interneurons and pyramidal cells in the rat hippocampus. Neuroscience 79:629–648.

Coetzee WA, Amarillo Y, Chiu J, Chow A, Lau D, McCormack T, Moreno H, Nadal MS, Ozaita A, Pountney D, Saganich M, Vega-Saenz dM, Rudy B. 1999. Molecular diversity of K^+ channels. Ann N Y Acad Sci 868: 233–285.

Connors BW, Gutnik MJ. 1990. Intrinsic firing patterns of diverse neocortical neurons. TINS 13:99–104.

Deans MR, Gibson JR, Sellitto C, Connors BW, Paul DL. 2001. Synchronous activity of inhibitory networks in neocortex requires electrical synapses containing connexin36. Neuron 31:477–485.

Faber ES, Sah P. 2002. Physiological role of calcium-activated potassium currents in the rat lateral amygdala. J Neurosci 22:1618–1628.

Freund TF. 2003. Interneuron diversity series: rhythm and mood in perisomatic inhibition. Trends Neurosci 26:489–495.

Fricker D, Miles R. 2001. Interneurons, spike timing, and perception. Neuron 32:771–774.

Fuller TA, Russchen FT, Price JL. 1987. Sources of presumptive glutamatergic/aspartergic afferents to the rat ventral striatopallidal region. J Comp Neurol 258:317–338.

Galarreta M, Hestrin S. 2002. Electrical and chemical synapses among parvalbumin fast-spiking GABAergic interneurons in adult mouse neocortex. Proc Natl Acad Sci U S A 99:12438–12443.

Gorelova N, Seamans JK, Yang CR. 2002. Mechanisms of dopamine activation of fast-spiking interneurons that exert inhibition in rat prefrontal cortex. J Neurophysiol 88:3150–3166.

Gupta A, Wang Y, Markram H. 2000. Organizing principles for a diversity of GABAergic interneurons and synapses in the neocortex. Science 287:273–278.

Halliwell JV, Adams PR. 1982. Voltage-clamp analysis of muscarinic excitation in hippocampal neurons. Brain Res 250:71–92.

Hestrin S, Galarreta M. 2005. Electrical synapses define networks of neocortical GABAergic neurons. Trends Neurosci 28:304–309.

Hormuzdi SG, Pais I, LeBeau FE, Towers SK, Rozov A, Buhl EH, Whittington MA, Monyer H. 2001. Impaired electrical signaling disrupts gamma frequency oscillations in connexin 36-deficient mice. Neuron 31:487–495.

Izhikevich EM. 2001. Resonate-and-fire neurons. Neural Netw 14:883–894.

Jacobowitz DM, Winsky L. 1991. Immunocytochemical localization of calretinin in the forebrain of the rat. J Comp Neurol 304:198–218.

Jefferys JGR, Traub RD, Whittington MA. 1996. Neuronal networks for induced "40 Hz" rhythms. Trends Neurosci 19:202–208.

Jonas P, Bischofberger J, Fricker D, Miles R. 2004. Interneuron Diversity series: fast in, fast out—temporal and spatial signal processing in hippocampal interneurons. Trends Neurosci 27:30–40.

Kawaguchi Y. 1993. Physiological, morphological, and histochemical characterization of three classes of interneurons in rat neostriatum. J Neurosci 13:4908–4923.

Kawaguchi Y. 1995. Physiological subgroups of nonpyramidal cells with specific morphological characteristics in layer II/III of rat frontal cortex. J Neurosci 15:2638–2655.

Kawaguchi Y, Kondo S. 2002. Parvalbumin, somatostatin and cholecystokinin as chemical markers for specific GABAergic interneuron types in the rat frontal cortex. J Neurocytol 31:277–287.

Kawaguchi Y, Kubota Y. 1993. Correlation of physiological subgroupings of nonpyramidal cells with parvalbumin- and calbindinD28k-immunoreactive neurons in layer V of rat frontal cortex. J Neurophysiol 70:387–396.

Kawaguchi Y, Kubota Y. 1997. GABAergic cell subtypes and their synaptic connections in rat frontal cortex. Cereb Cortex 7:476–486.

Kawaguchi Y, Kubota Y. 1998. Neurochemical features and synaptic connections of large physiologically-identified GABAergic cells in the rat frontal cortex. Neuroscience 85:677–701.

Kemppainen S, Pitkänen A. 2000. Distribution of parvalbumin, calretinin, and calbindin-D(28k) immunoreactivity in the rat amygdaloid complex and colocalization with gamma-aminobutyric acid. J Comp Neurol 426: 441–467.

Kroner S, Rosenkranz JA, Grace AA, Barrionuevo G. 2005. Dopamine modulates excitability of basolateral amygdala neurons in vitro. J Neurophysiol 93:1598–1610.

Levita L, Mania I, Rainnie DG. 2003a. Dopamine activates multiple conductances in the basolateral amygdala. Soc Neurosci Abstr 30:336.19.

Levita L, Mania I, Rainnie DG. 2003b. Subtypes of substance P receptor immunoreactive interneurons in the rat basolateral amygdala. Brain Res 981:41–51.

Llinas RR. 1988. The intrinsic electrophysiological properties of mammalian neurons: insights into central nervous system function. Science 242:1654–1664.

Ludwig A, Zong X, Jeglitsch M, Hofmann F, Biel M. 1998. A family of hyperpolarization-activated mammalian cation channels. Nature 393: 587–591.

Maccaferri G, Roberts JD, Szucs P, Cottingham CA, Somogyi P. 2000. Cell surface domain specific postsynaptic currents evoked by identified GABAergic neurones in rat hippocampus in vitro. J Physiol 524:91–116.

Mahanty NK, Sah P. 1998. Calcium-permeable AMPA receptors mediate long-term potentiation in interneurons in the amygdala. Nature 394: 683–687.

Markram H, Toledo-Rodriguez M, Wang Y, Gupta A, Silberberg G, Wu C. 2004. Interneurons of the neocortical inhibitory system. Nat Rev Neurosci 5:793–807.

Mascagni F, McDonald AJ. 2003. Immunohistochemical characterization of cholecystokinin containing neurons in the rat basolateral amygdala. Brain Res 976:171–184.

McBain CJ, Fisahn A. 2001. Interneurons unbound. Nat Rev Neurosci 2:11–23.

McCormick DA, Pape H. 1990. Properties of a hyperpolarization-activated cation current and its role in rhythmic oscillation in thalamic relay neurones. J Physiol 431:291–318.

McCormick DA, Connors BW, Lighthall JW, Prince DA. 1985. Comparative electrophysiology of pyramidal and sparsely spiny stellate neurons of the neocortex. J Neurophysiol 54:782–806.

McDonald AJ. 1982. Neurons of the lateral and basolateral amygdaloid nuclei: a Golgi study in the rat. J Comp Neurol 212:293–312.

McDonald AJ. 1989. Coexistence of somatostatin with neuropeptide Y, but not with cholecystokinin or vasoactive intestinal peptide, in neurons of the rat amygdala. Brain Res 500:37–45.

McDonald AJ. 1992. Projection neurons of the basolateral amygdala: a correlative Golgi and retrograde tract tracing study. Brain Res Bull 28:179–185.

McDonald AJ. 1996. Glutamate and aspartate immunoreactive neurons of the rat basolateral amygdala: colocalization of excitatory amino acids and projections to the limbic circuit. J Comp Neurol 365:367–379.

McDonald AJ, Betette RL. 2001. Parvalbumin-containing neurons in the rat basolateral amygdala: morphology and co-localization of Calbindin-D(28k). Neuroscience 102:413–425.

McDonald AJ, Culberson JL. 1981. Neurons of the basolateral amygdala: a Glogi study in the opposum (*Didelphis virginiana*). Am J Anat 162: 327–342.

McDonald AJ, Mascagni F. 2001a. Colocalization of calcium-binding proteins and GABA in neurons of the rat basolateral amygdala. Neuroscience 105:681–693.

McDonald AJ, Mascagni F. 2001b. Localization of the CB1 type cannabinoid receptor in the rat basolateral amygdala: high concentrations in a subpopulation of cholecystokinin-containing interneurons. Neuroscience 107:641–52.

McDonald AJ, Mascagni F. 2002. Immunohistochemical characterization of somatostatin containing interneurons in the rat basolateral amygdala. Brain Res 943:237–244.

McDonald AJ, Mascagni F. 2004. Parvalbumin-containing interneurons in the basolateral amygdala express high levels of the alpha1 subunit of the GABAA receptor. J Comp Neurol 473:137–146.

McDonald AJ, Mascagni F. 2006. Differential expression of Kv3.1b and Kv3.2 potassium channel subunits in interneurons of the basolateral amygdala. Brain Res (in press).

McDonald AJ, Pearson JC. 1989. Coexistence of GABA and peptide immunoreactivity in non-pyramidal of the basolateral amygdala. Neurosci Lett 100:53–58.

McDonald AJ, Mascagni F, Mania I, Rainnie DG. 2005. Evidence for a perisomatic innervation of parvalbumin-containing interneurons by individual pyramidal cells in the basolateral amygdala. Brain Res 1035:32–40.

Miles R, Toth K, Gulyas AI, Hajos N, Freund TF. 1996. Differences between somatic and dendritic inhibition in the hippocampus. Neuron 16:815–823.

Millhouse OE, DeOlmos J. 1983. Neuronal configurations in lateral and basolateral amygdala. Neuroscience 10:1269–1300.

Muller JF, Mascagni F, McDonald AJ. 2003. Synaptic connections of distinct interneuronal subpopulations in the rat basolateral amygdalar nucleus. J Comp Neurol 456:217–236.

Muller JF, Mascagni F, McDonald AJ. 2005. Coupled networks of parvalbumin-immunoreactive interneurons in the rat basolateral amygdala. J Neurosci 25:7366–7376.

Muller JF, Mascagni F, McDonald AJ. 2006. Pyramidal cells of the rat basolateral amygdala: synaptology and innervation by parvalbumin-immunoreactive interneurons. J Comp Neurol 494:635–650.

Nelson S. 2002. Cortical microcircuits: diverse or canonical? Neuron 36: 19–27.

Pape HC, Driesang RB. 1998. Ionic mechanisms of intrinsic oscillations in neurons of the basolateral amygdaloid complex. J Neurophysiol 79: 217–226.

Pare D, Royer S, Smith Y, Lang EJ. 2003. Contextual inhibitory gating of impulse traffic in the intra-amygdaloid network. Ann N Y Acad Sci 985:78–91.

Parra P, Gulyas AI, Miles R. 1998. How many subtypes of inhibitory cells in the hippocampus? Neuron 20:983–993.

Pawelzik H, Bannister AP, Deuchars J, Ilia M, Thomson AM. 1999. Modulation of bistratified cell IPSPs and basket cell IPSPs by pentobarbitone sodium, diazepam and Zn^{2+}: dual recordings in slices of adult rat hippocampus. Eur J Neurosci 11:3552–3564.

Pawelzik H, Hughes DI, Thomson AM. 2002. Physiological and morphological diversity of immunocytochemically defined parvalbumin- and cholecystokinin-positive interneurones in CA1 of the adult rat hippocampus. J Comp Neurol 443:346–367.

Pelletier JG, Pare D. 2004. Role of amygdala oscillations in the consolidation of emotional memories. Biol Psychiatry 55:559–562.

Pitkänen A, Amaral DG. 1993. Distribution of parvalbumin-immunoreactive cells and fibers in the monkey temporal lobe: the amygdaloid complex. J Comp Neurol 331:14–36.

Pitkänen A, Amaral DG. 1994. The distribution of GABAergic cells, fibers, and terminals in the monkey amygdaloid complex: an immunohistochemical and in situ hybridization study. J Neurosci 14:2200–2224.

Pitkänen A, Kemppainen S. 2002. Comparison of the distribution of calcium-binding proteins and intrinsic connectivity in the lateral nucleus of the rat, monkey, and human amygdala. Pharmacol Biochem Behav 71:369–377.

Ponomarenko AA, Korotkova TM, Haas HL. 2003. High frequency (200 Hz) oscillations and firing patterns in the basolateral amygdala and dorsal endopiriform nucleus of the behaving rat. Behav Brain Res 141:123–129.

Pouille F, Scanziani M. 2001. Enforcement of temporal fidelity in pyramidal cells by somatic feed-forward inhibition. Science 293:1159–1163.

Rainnie DG. 1999a. Serotonergic modulation of neurotransmission in the rat basolateral amygdala. J Neurophysiol 82:69–85.

Rainnie DG. 1999b. Synchronous inhibitory synaptic potentials in simultaneously recorded neurons of the basolateral amygdala. Soc Neurosci Abstr 26:651.

Rainnie DG, Fernhout B-JH, Shinnick-Gallagher P. 1992. Differential actions of corticotropin releasing factor on basolateral and central amygdaloid neurones, in vitro. J Pharmacol Exp Ther 263:846–858.

Rainnie DG, Asprodini EK, Shinnick-Gallagher P. 1993. Intracellular recordings from morphologically identified neurons of the basolateral amygdala. J Neurophysiol 69:1350–1361.

Rainnie DG, Holmes KH, Shinnick-Gallagher P. 1994. Activation of postsynaptic metabotropic glutamate receptors by *trans*-ACPD hyperpolarizes neurons of the basolateral amygdala. J Neurosci 14:7208–7220.

Rainnie DG, Bergeron R, Sajdyk TJ, Patil M, Gehlert DR, Shekhar A. 2004. Corticotrophin releasing factor-induced synaptic plasticity in the amygdala translates stress into emotional disorders. J Neurosci 24: 3471–3479.

Rodriguez E, George N, Lachaux JP, Martinerie J, Renault B, Varela FJ. 1999. Perception's shadow: long-distance synchronization of human brain activity. Nature 397:430–433.

Rosenkranz JA, Grace AA. 1999. Modulation of basolateral amygdala neuronal firing and afferent drive by dopamine receptor activation in vivo. J Neurosci 19:11027–11039.

Rosenkranz JA, Grace AA. 2001. Dopamine attenuates prefrontal cortical suppression of sensory inputs to the basolateral amygdala of rats. J Neurosci 21:4090–4103.

Rosenkranz JA, Grace AA. 2002. Dopamine-mediated modulation of odour-evoked amygdala potentials during pavlovian conditioning. Nature 417:282–287.

Rudy B. 1988. Diversity and ubiquity of K channels. Neuroscience 25:729–749.

Rudy B, McBain CJ. 2001. Kv3 channels: voltage-gated K^+ channels designed for high-frequency repetitive firing. Trends Neurosci 24:517–526.

Santoro B, Chen S, Luthi A, Pavlidis P, Shumyatsky GP, Tibbs GR, Siegelbaum SA. 2000. Molecular and functional heterogeneity of hyperpolarization-activated pacemaker channels in the mouse CNS. J Neurosci 20:5264–5275.

Seidenbecher T, Laxmi TR, Stork O, Pape HC. 2003. Amygdalar and hippocampal theta rhythm synchronization during fear memory retrieval. Science 301:846–850.

Sik A, Tamamaki N, Freund TF. 1993. Complete axon arborization of a single CA3 pyramidal cell in the rat hippocampus, and its relationship with postsynaptic parvalbumin-containing interneurons. Eur J Neurosci 5:1719–1728.

Singer W. 2001. Consciousness and the binding problem. Ann N Y Acad Sci 929:123–146.

Smith Y, Pare JF, Pare D. 1998. Cat intraamygdaloid inhibitory network: ultrastructural organization of parvalbumin-immunoreactive elements. J Comp Neurol 391:164–179.

Smith Y, Pare JF, Pare D. 2000. Differential innervation of parvalbumin-immunoreactive interneurons of the basolateral amygdaloid complex by cortical and intrinsic inputs. J Comp Neurol 416:496–508.

Somogyi P, Kisvarday ZF, Martin KA, Whitteridge D. 1983. Synaptic connections of morphologically identified and physiologically characterized large basket cells in the striate cortex of cat. Neuroscience 10:261–294.

Sorvari H, Soininen H, Paljärvi L, Karkola K, Pitkänen A. 1995. Distribution of parvalbumin-immunoreactive cells and fibers in the human amygdaloid complex. J Comp Neurol 360:185–212.

Sorvari H, Soininen H, Pitkänen A. 1996. Calretinin-immunoreactive cells and fibers in the human amygdaloid complex. J Comp Neurol 369:188–208.

Tamas G, Buhl EH, Lorincz A, Somogyi P. 2000. Proximally targeted GABAergic synapses and gap junctions synchronize cortical interneurons. Nat Neurosci 3:366–371.

Thomson AM, Bannister AP, Hughes DI, Pawelzik H. 2000. Differential sensitivity to zolpidem of IPSPs activated by morphologically identified CA1 interneurons in slices of rat hippocampus. Eur J Neurosci 12:425–436.

Toledo-Rodriguez M, Blumenfeld B, Wu C, Luo J, Attali B, Goodman P, Markram H. 2004. Correlation maps allow neuronal electrical properties to be predicted from single-cell gene expression profiles in rat neocortex. Cereb Cortex 14:1310–1327.

Traub RD, Miles R, Buzsáki G. 1992. Computer simulation of carbachol-driven rhythmic population oscillations in the CA3 region of the in vitro rat hippocampus. J Physiol 451:653–672.

Varela F, Lachaux JP, Rodriguez E, Martinerie J. 2001. The brainweb: phase synchronization and large-scale integration. Nat Rev Neurosci 2:229–239.

Wang Y, Gupta A, Toledo-Rodriguez M, Wu CZ, Markram H. 2002. Anatomical, physiological, molecular and circuit properties of nest basket cells in the developing somatosensory cortex. Cereb Cortex 12:395–410.

Washburn MS, Moises HC. 1992a. Muscarinic responses of rat basolateral amygdaloid neurons recorded in vitro. J Physiol 449:121–154.

Washburn MS, Moises HC. 1992b. Electrophysiological and morphological properties of rat basolateral amygdaloid neurons in vitro. J Neurosci 12:4066–4079.

Womble MD, Moises HC. 1992. Muscarinic inhibition of M-current and a potassium leak conductance in neurones of the rat basolateral amygdala. J Physiol 457:93–114.

Yamaguchi Y, Aota Y, Sato N, Wagatsuma H, Wu Z. 2004. Synchronization of neural oscillations as a possible mechanism underlying episodic memory: a study of theta rhythm in the hippocampus. J Integr Neurosci 3:143–157.